REPORT DOCUMENTATION PAGE

Form Approved
OMB No. 0704-0188

1. REPORT DATE *(DD-MM-YYYY)*	2. REPORT TYPE	3. DATES COVERED *(From - To)*
01-08-2010	Final Performance	April 1, 2007 - July 31, 2010

4. TITLE AND SUBTITLE
Performance Characterization of Polyimide-Carbon Fiber Composites for Future Hypersonic Vehicles

5a. CONTRACT NUMBER
C07-00449

5b. GRANT NUMBER
FA9550-07-1-0285

5c. PROGRAM ELEMENT NUMBER
N/A

6. AUTHOR(S)
Dr. Jaime C. Grunlan, Co-PI's Dr. K.R. Rajagopal and Dr. J.N. Reddy

5d. PROJECT NUMBER
32525-38390

5e. TASK NUMBER
N/A

5f. WORK UNIT NUMBER
N/A

7. PERFORMING ORGANIZATION NAME(S) AND ADDRESS(ES)
Texas Engineering Experiment Station
3000 TAMUS
College Station, TX 77843-3000

8. PERFORMING ORGANIZATION REPORT NUMBER
081710

9. SPONSORING/MONITORING AGENCY NAME(S) AND ADDRESS(ES)
Air Force Office of Scientific Research
875 N Randolph St
Suite 325
Arlington, VA 22203

10. SPONSOR/MONITOR'S ACRONYM(S)
AFOSR

11. SPONSORING/MONITORING AGENCY REPORT NUMBER

12. DISTRIBUTION AVAILABILITY STATEMENT

13. SUPPLEMENTARY NOTES

14. ABSTRACT

The Air Force, Army, and Navy have initiated research and development progress to develop hypersonic vehicles in the Mach 5-15 range. Two broad categories are being considered, namely: (i) vehicles that fly at low altitudes for short times (minutes) over distances of hundreds of miles and (ii) flights that are global and cover lower space orbits over periods of hours. Specifically, the Air Force for future vehicles need to be able to reach anywhere in the world in one hour (Vista 25 program). The aerodynamic heating of the vehicle exterior depends on the altitude, but generally exterior vehicle temperatures are proportional to the square of the Mach number. The primary structures of hypersonic vehicles need to be lightweight, strong and thermally durable for the duration of the flight (or for multiple flights in the case of reusable vehicles). Transition-metal carbides, referred to as ultra-high temperature (UHT) materials, are interesting because they are refractory materials with the highest known melting points (that in many cases exceed 2600°C). Applications for UHT materials such as hypersonic flight, atmospheric re-entry, and rocket propulsion, with temperatures exceeding 3000°C, challenge the survivability of many known materials currently in use. Unfortunately, the synthesis of the refractory transition-metal carbides requires high temperatures that can exceed 1700°C. The in-situ synthesis of transition-metal carbides, in an argon atmosphere using transition-metal halide salts solution-processed with polymer matrices, is described here as a low temperature method for making UHT carbides. For example, tantalum carbide (Tm = 3880°C) can be produced at temperatures as low as 1000°C with high yield (>80%). This relatively low temperature procedure is relatively universal in terms of the variety of transition metals (Ta, Hf, Nb, etc.) that can be used, making it very useful for a wide variety of high temperature applications. The AFR-PEPA-N polyimide-carbon fiber composite

system developed by AFRL and AFOSR sponsored programs is the leading candidate as the starting material for this conversion process. This polymer system is already being processed for leading edge primary structures and engine components for present and future stealth aircraft. In addition to describing our work to generate carbide from this high temperature polymer system, work to understand the extreme service environments and associated multiple mechanical, thermal, chemical and physical degradation mechanisms on hypersonic vehicle performance capabilities for AFR-PEPA-N-carbon fiber composites will be briefly described. A sequential degradation model based on experimental data on each mechanism is also being developed as part of this project.

15. SUBJECT TERMS

16. SECURITY CLASSIFICATION OF:			**17. LIMITATION OF ABSTRACT**	**18. NUMBER OF PAGES**	**19a. NAME OF RESPONSIBLE PERSON**
			UU	1	Jaime C. Grulan
a. REPORT	**b. ABSTRACT**	**c. THIS PAGE**			**19b. TELEPONE NUMBER (*Include area code)***
U	U	U			979-845-3027

INSTRUCTIONS FOR COMPLETING SF 298

1. REPORT DATE. Full publication date, including day, month, if available. Must cite at lest the year and be Year 2000 compliant, e.g., 30-06-1998; xx-08-1998; xx-xx-1998.

2. REPORT TYPE. State the type of report, such as final, technical, interim, memorandum, master's thesis, progress, quarterly, research, special, group study, etc.

3. DATES COVERED. Indicate the time during which the work was performed and the report was written, e.g., Jun 1997 - Jun 1998; 1-10 Jun 1996; May - Nov 1998; Nov 1998.

4. TITLE. Enter title and subtitle with volume number and part number, if applicable. On classified documents, enter the title classification in parentheses.

5a. CONTRACT NUMBER. Enter all contract numbers as they appear in the report, e.g. F33615-86-C-5169.

5b. GRANT NUMBER. Enter all grant numbers as they appear in the report, e.g. 1F665702D1257.

5c. PROGRAM ELEMENT NUMBER. Enter all program element numbers as they appear in the report, e.g. AFOSR-82-1234.

5d. PROJECT NUMBER. Enter al project numbers as they appear in the report, e.g. 1F665702D1257; ILIR.

5e. TASK NUMBER. Enter all task numbers as they appear in the report, e.g. 05; RF0330201; T4112.

5f. WORK UNIT NUMBER. Enter all work unit numbers as they appear in the report, e.g. 001; AFAPL30480105.

6. AUTHOR(S). Enter name(s) of person(s) responsible for writing the report, performing the research, or credited with the content of the report. The form of entry is the last name, first name, middle initial, and additional qualifiers separated by commas, e.g. Smith, Richard, Jr.

7. PERFORMING ORGANIZATION NAME(S) AND ADDRESS(ES). Self-explanatory.

8. PERFORMING ORGANIZATION REPORT NUMBER. Enter all unique alphanumeric report numbers assigned by the performing organization, e.g. BRL-1234; AFWL-TR-85-4017-Vol-21-PT-2.

9. SPONSORING/MONITORS AGENCY NAME(S) AND ADDRESS(ES). Enter the name and address of the organization(s) financially responsible for and monitoring the work.

10. SPONSOR/MONITOR'S ACRONYM(S). Enter, if available, e.g. BRL, ARDEC, NADC.

11. SPONSOR/MONITOR'S REPORT NUMBER(S). Enter report number as assigned by the sponsoring/ monitoring agency, if available, e.g. BRL-TR-829; -215.

12. DISTRIBUTION/AVAILABILITY STATEMENT. Use agency-mandated availability statements to indicate the public availability or distribution limitations of the report. If additional limitations/restrictions or special markings are indicated, follow agency authorization procedures, e.g. RD/FRD, PROPIN, ITAR, etc. Include copyright information.

13. SUPPLEMENTARY NOTES. Enter information not included elsewhere such as: prepared in cooperation with; translation of; report supersedes; old edition number, etc.

14. ABSTRACT. A brief (approximately 200 words) factual summary of the most significant information.

15. SUBJECT TERMS. Key words or phrases identifying major concepts in the report.

16. SECURITY CLASSIFICATION. Enter security classification in accordance with security classification regulations, e.g. U, C, S, etc. If this form contains classified information, stamp classification level on the top and bottom of this page.

17. LIMITATION OF ABSTRACT. This block must be completed to assign a distribution limitation to the abstract. Enter UU (Unclassified Unlimited) or SAR (Same as Report). An entry in this block is necessary if the abstract is to be limited.

FINAL REPORT
TO
AIR FORCE OFFICE OF SCIENTIFIC RESEARCH

PERFORMANCE CHARACTERIZATION OF POLYIMIDE-CARBON FIBER COMPOSITES FOR FUTURE HYPERSONIC VEHICLES

PI
Dr. Jaime C. Grunlan

Co-PIs
Dr. K. R. Rajagopal
Dr. J. N. Reddy

Texas A&M University

August 2010

AFOSR CONTRACT NO.:
FA 9550-07-1-0285

1 OBJECTIVES

- The overall goals of this program are to conduct fundamental studies to ascertain the multiple mechanical, thermal, chemical, and physical degradation mechanisms on hypersonic vehicle performance capabilities for AFR-PEPA-4 polyimide carbon fiber composites for lightweight structural applications for such vehicles.
- The individual fundamental service environment-induced degradation mechanisms include:
  - further polyimide crosslinking;
  - oxidative composite surface degradation;
  - composite strength and modulus decreases with increasing thermal exposure;
  - moisture-induced composite blistering;
  - ablation/spalling induced composite shock wave damages.
- The further curing of AFR-PEPA-4 polyimides has an effect on the resins mechanical properties as a result of aerodynamic heating during hypersonic flight that will be characterized and then incorporated into the overall damage accumulation model.
- The damage growth kinetics based on the interconnection between fundamental oxidative chemical degradation, composite microcrack growth characteristics and hypersonic vehicle service environment conditions will be developed in a series of generic phase diagrams that can be fed into the damage growth composite strength and modulus modeling task.
- The hypersonic vehicle thermal and stress imposed service environments on carbon fiber, transverse composite and matrix failure temperatures in the absence of oxidative degradation will be characterized and time-temperature-mechanical property diagrams will be developed.
- Characterization of hygrothermal-induced composite damage will be determined by blister formation.
- It will be ascertained if rapid heating and the associated weight loss of composites in hypersonic vehicle service environments can result in shock wave-induced composite damage.
- A time dependent damage model will be developed to address through thickness damage zones of structural and mechanical properties ranging from an exterior chemical degradation, oxidative, brittle char zone through to inner zones with little chemical degradation but lower strengths and modulus as a result from increased temperature exposure.

- The ultimate objective is to develop a generic lifetime performance model for AFR-PEPA-4 carbon fiber composites exposed to hypersonic vehicle service environments based on synergistic, fundamental, diverse thermal, chemical, physical, and mechanical potential damage mechanisms.

2 STATUS OF EFFORT

In the third and final year of the program the following technical areas were pursued and their progress is reported:

(i) Further AFR-PEPA-4 polyimide cross-linking;
(ii) Oxidative surface degradation of AFR-PEPA-4 carbon fiber composites;
(iii) Composite strength and modulus decreases with increasing thermal exposure, that includes resin, fiber and fiber-matrix interface deterioration in mechanical properties;
(iv) Moisture-induced composite blistering;
(v) Ablation/spalling induced composite damage as a result of shock waves;
(vi) Development of a model within a general thermodynamic framework to describe various types of damage in High Temperature Polymer Composites.

3 ACCOMPLISHMENTS/NEW FINDINGS

3.1 FURTHER AFR-PEPA-4 POLYIMIDE CROSS-LINKING

AFR-PEPA-N polyimide only obtains 80% cure through the phenylethynyl crosslinking carbon triple bonds under the standard cure cycle of 375 °C for 4 hours [1]. During the initial stages of hypersonic flight, aerodynamic heating will induce additional cure of the exterior layers of the composite. However, this further rapid curing will result in an increase of the polyimide crosslinking and T_g that will affect the resin's mechanical properties.

FTIR and DSC studies, as a function of isothermal cure, for AFR-PEPA-4 polyimides reveal that full cure is still not obtained for a cure cycle of 410 °C for 8 hours [1]. In Figure 1, a plot of T_g versus reaction conversion is shown. It was determined that full cure can be achieved at 437.2 °C by extrapolation of this plot. For cure lines at 440 – 450 °C of over an hour, the major degradation regime will be shifted into the cure region. The mechanical properties of the AFR-PEPA-N polyimides can be effected by the combination of crosslink density, T_g and degradation mechanisms, which have not yet been determined as a function of temperature and cure conditions. Characterization of the time-temperature-mechanical property (T.T.M.P.) relationships in the 400 - 500 °C temperature range for AFR-PEPA-N polyimide is currently underway.

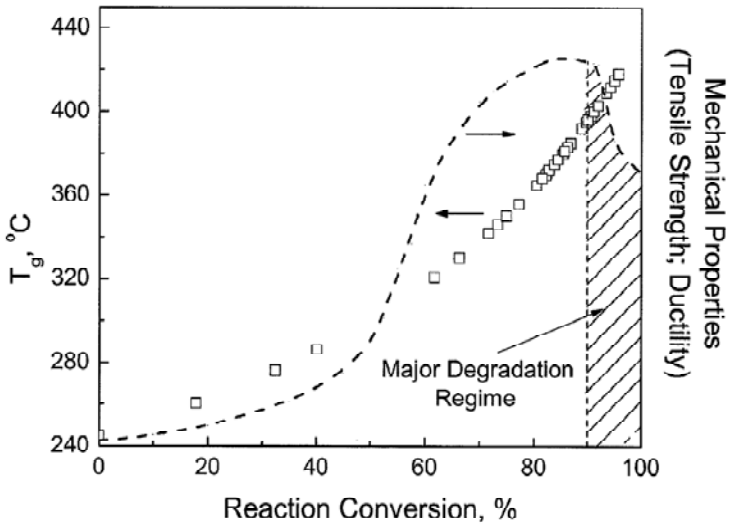

Figure 1: T_g as a function of reaction conversion for AFR-PEPA-4 polyimide

The AFR-PEPA-N polyimide resin panels have been successfully made, cut for samples, and tested. The pieces were subjected to the temperatures of 410, 440, 470, and 500 °C with exposure times of 30 minutes, 1, 2, 4, and 8 hours. A TA instrument, Q20, differential scanning calorimetry (DSC) and a Q800 dynamic mechanical analyzer (DMA) was used to measure the T_g's of each sample, a Q50 thermogravimetric analyzer (TGA) was used to measure the T_d's, and an Instron was used to determine the elastic modulus and tensile strength. The small (~2-3 mm) sample squares used for the DSC and TGA were further cured in the instruments before conducting test to obtain the glass transition, melting, or decomposition temperature. The rectangular samples for the DMA and Instron were further cured in a preheated furnace oven with a nitrogen atmosphere.

Figure 2(a) shows the glass transition temperatures as a function of cure time in relation to the cure temperatures for the polyimide resin. The 410 °C temperature run showed the best linear trend as cure time was increased, with 8 hours resulting in the highest T_g (458 °C). While the 440 and 470 °C cure temperatures gave high T_g's for 0.5 and 1 hour cure times, the T_g's became increasingly higher with some of the cure times resulting in an undeterminable T_g from the data. The 2 and 4 hour cure times resulted in T_g's around 500 °C for the 440 °C cure temperature. Beyond 2 hours for the 470 °C cure condition, the T_g's were indistinguishable and samples visually showed signs that degradation had started to occur. Despite the high T_g (530 °C) for the 500 °C 30 minute curing, the sample visually appeared to be degraded on the exterior. This data suggests that the cure conditions need to be any cure time at 410 °C or less than two hours for cure temperatures below 470 °C. The melting temperatures as a function of cure time in relation to the cure temperatures are shown in Figure 2(b). There was not as much variability in T_m as there was for the T_g, but the T_m's decreased slightly as the cure time was increased regardless of curing condition. This increase in T_g is a result of restriction of chain mobility caused by a greater crosslinked structure. Based on the results obtained in Figure 2,

the four hour at 440 °C cure resulted in the best combination of glass transition and melting temperature.

Weight loss during cure, decomposition temperature (T_d), and char yield were also obtained for the further cured resin. Figure 3 shows the weight loss during cure as a function of cure time with respect to the cure temperature. The TGA was used to first cure the samples and then heated further to obtain the T_d's. The 410 °C curing temperature showed little weight loss (< 2.4%), even with 8hr curing time. Both the 410 and 440 °C curing temperatures showed linear weight loss trends as the curing time was increased, while the 470 and 500 °C curing temperatures exhibited a logarithmic trend with significant weight loss (> 10%) for cure times > 2 hours for 470 °C and all cure times for 500 °C. These trends are expected, in particular with the higher cure temperatures, due to the eventual overlap of continued crosslinking and degradation. The decomposition temperature trends are similar to the weight loss during cure except that the 470 °C cure temperature exhibits a linear trend, as shown in Figure 4. The difference in T_d's for each cure temperature from 30 minutes to 8 hours nearly doubled with each 30 °C cure temperature increment. While having a high T_d is beneficial, the amount of weight loss during cure for those samples with higher T_d's is too great for using those cure temperatures/times for post curing conditions.

The tensile strength (Fig. 5(a)) and elastic modulus (Fig. 5(b)) were measured for each of the polyimide resin cure times/temperatures. The 410 °C cure temperature, regardless of cure time, maintained the best elastic modulus and tensile strength properties. Cure times less than four hours at 440 °C maintained moderate elastic modulus and tensile strength despite being lower than the 410 °C cure temperature/times. Curing at 470 °C for 8 hr and > 30 minutes at 500 °C resulted in samples that were too brittle or degraded to be tested. Based on these results, curing 8 hours at 410 °C produces the best mechanical properties (E ~ 2.1 GPa and TS ~ 45 MPa).

Optical microscope images for five selected further cured samples are shown in Figure 6 based on the thermal and mechanical properties results. Two samples, cured at 410 °C for 30 minutes (Fig. 6(a)) and 8 hours (Fig. 6(b)), suggest that there are still regions of uncrosslinked material due to the brighter brown areas. The sample cured one hour at 440 °C (Fig. 6(c)) was selected in order to determine if sample maintained structural integrity on the micro scale. This cure time/temperature condition shows remaining uncrosslinked material, but also indicates no significant degradation occurred. Figure 6(d) and (e) are the 30 minute cure time at 470 and 500 °C curing temperatures, respectively. These samples not only showed major degradation from the optical images, but also appeared to be degraded to the naked eye. All of the optical images in Figure 6 verify that the lower curing temperatures are better for obtaining a further cured sample that maintains structural integrity.

Figure 7 shows the results obtained from ATR FTIR for the same samples used for the optical images. With increasing cure time/temperature, the intensity of carbon double (1640-1680 cm^{-1}) and single bonds (800-1300 cm^{-1}) increases, indicating further crosslinking of the triple bonds (2100-2260 cm^{-1}). As the cure temperature is raised to 470 °C, these bond intensities begin to drop due to degradation, which is

expected based on the thermal and mechanical property data. There is a small presence of triple bonds still remaining for both of the 410 °C samples, which is also suggested by the lower intensity of the carbon double and single bonds. The 500 °C sample lacks the appearance of major chemical bond shifts due to the severity of degradation that occurred.

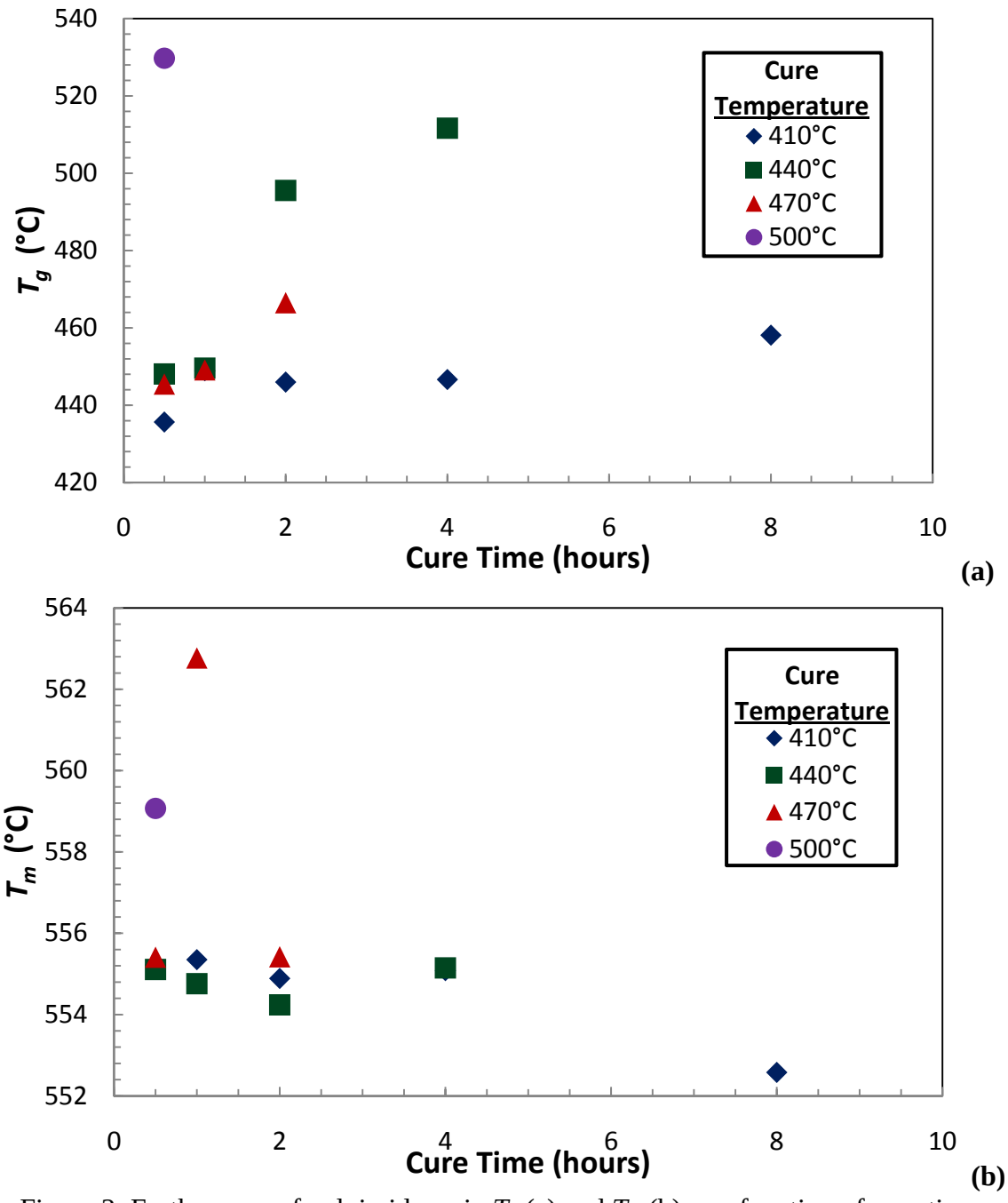

Figure 2: Further cure of polyimide resin T_g (a) and T_m (b) as a function of cure time (hours) and temperature (°C).

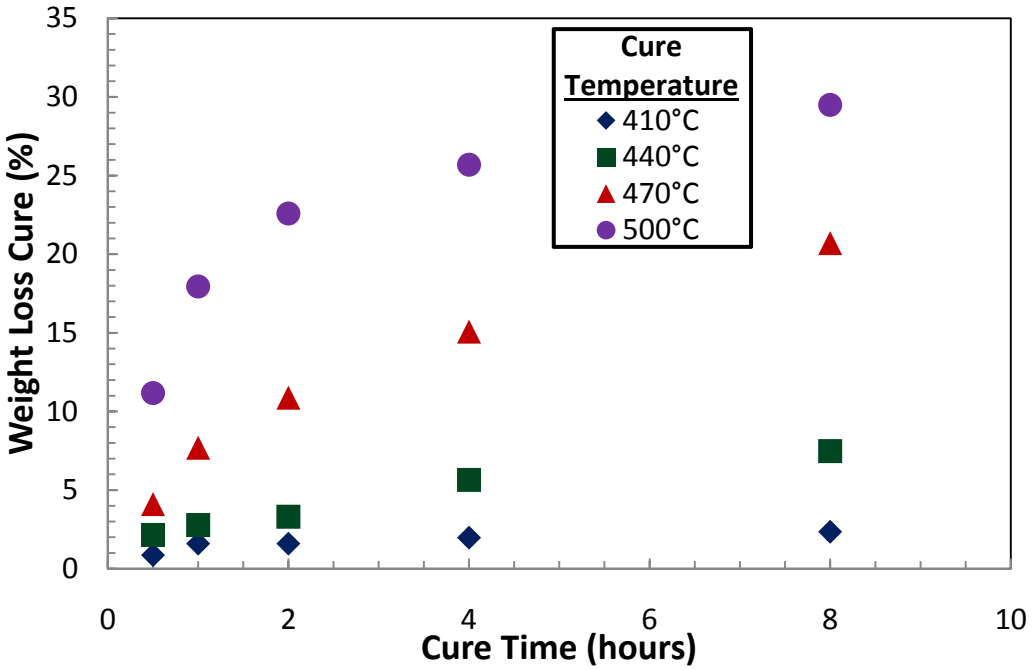

Figure 3: Amount of weight loss (%) as a function of cure time (hours) and temperature (°C) occurring during further cure of polyimide resin.

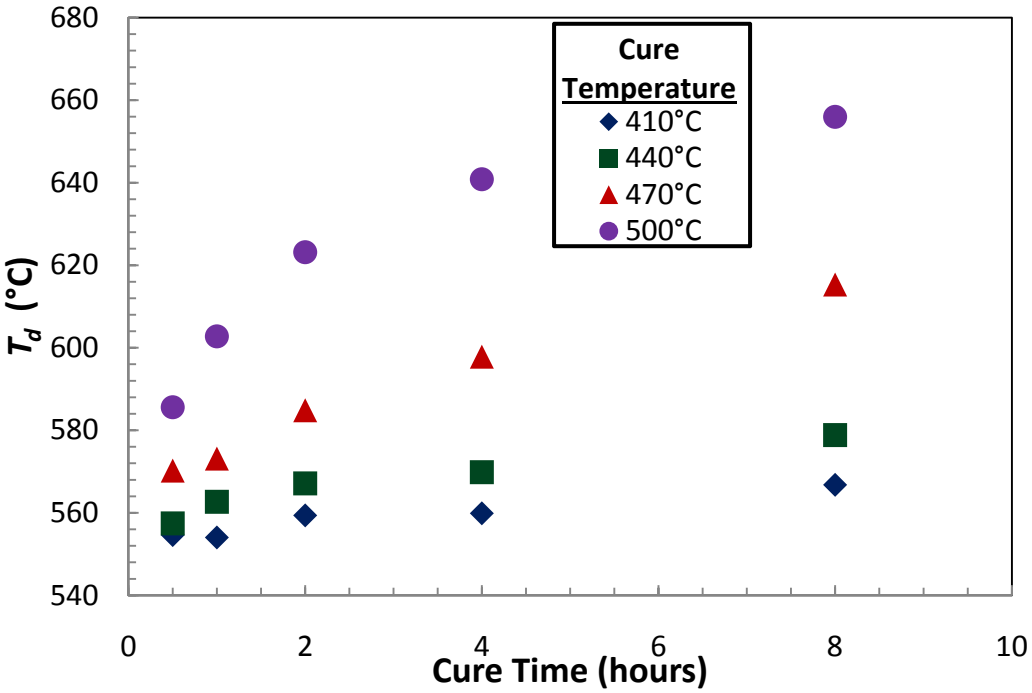

Figure 4: Decomposition temperature, T_d, (°C) as a function of cure time (hours) and temperature (°C) occurring during further cure of polyimide resin.

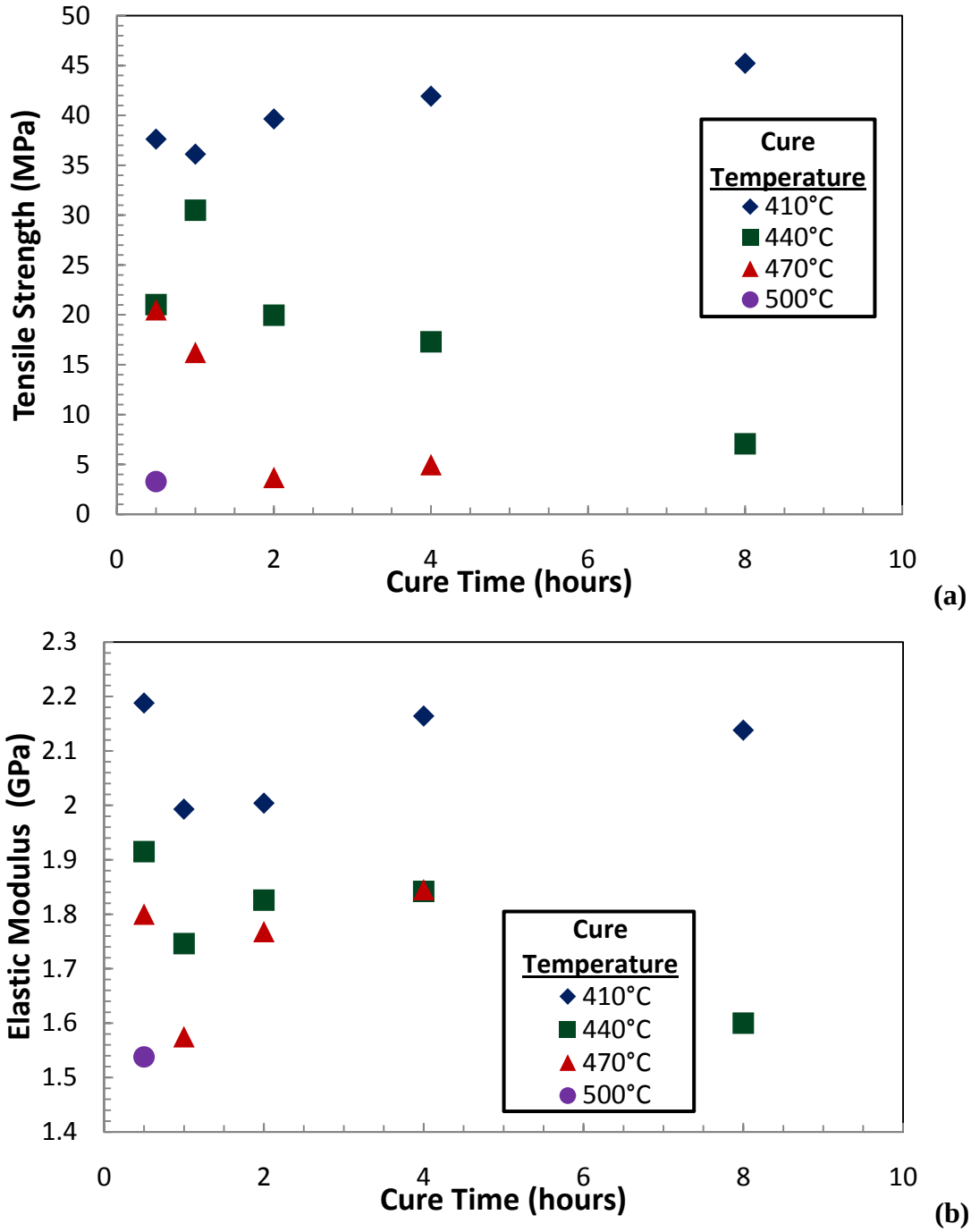

Figure 5: Further cure of polyimide resin's tensile strength (a) and elastic modulus (b) as a function of cure time (hours) and temperature (°C).

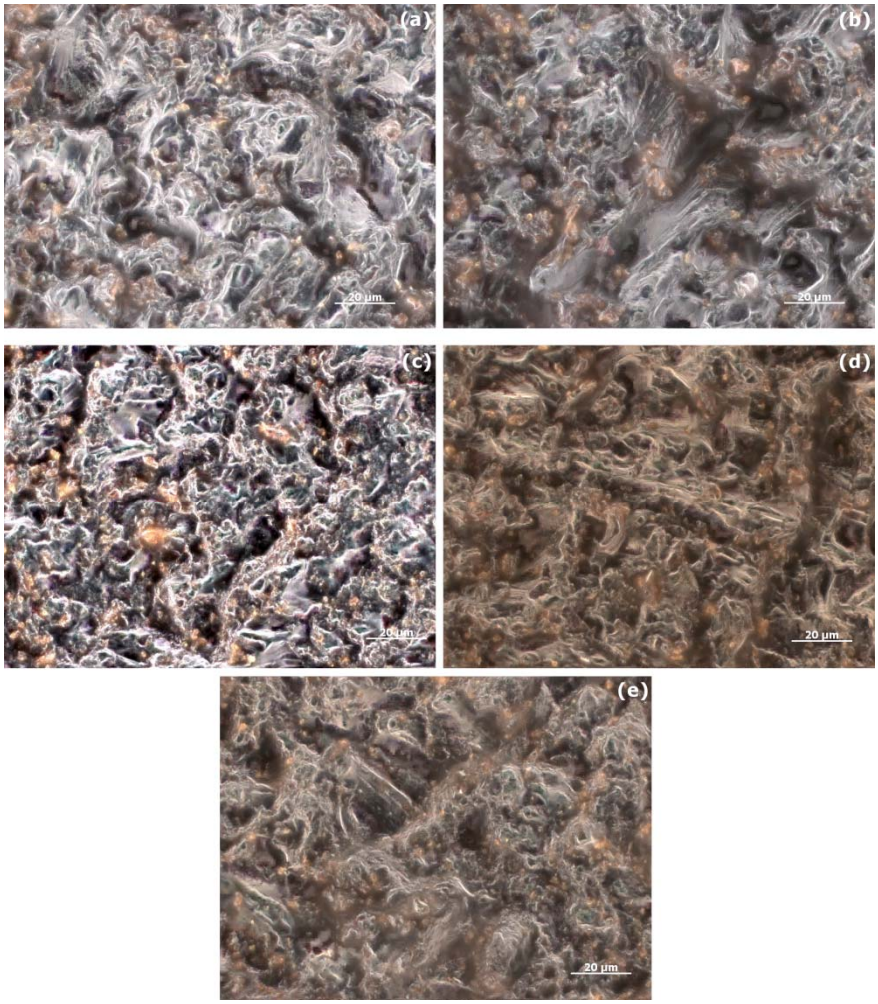

Figure 6: Polyimide resin cured for 30 min at 410 °C (a), 8 hours at 410 °C (b), 1 hour at 440 °C (c), 30 min at 470 °C (d), and 30 min at 500 °C (e).

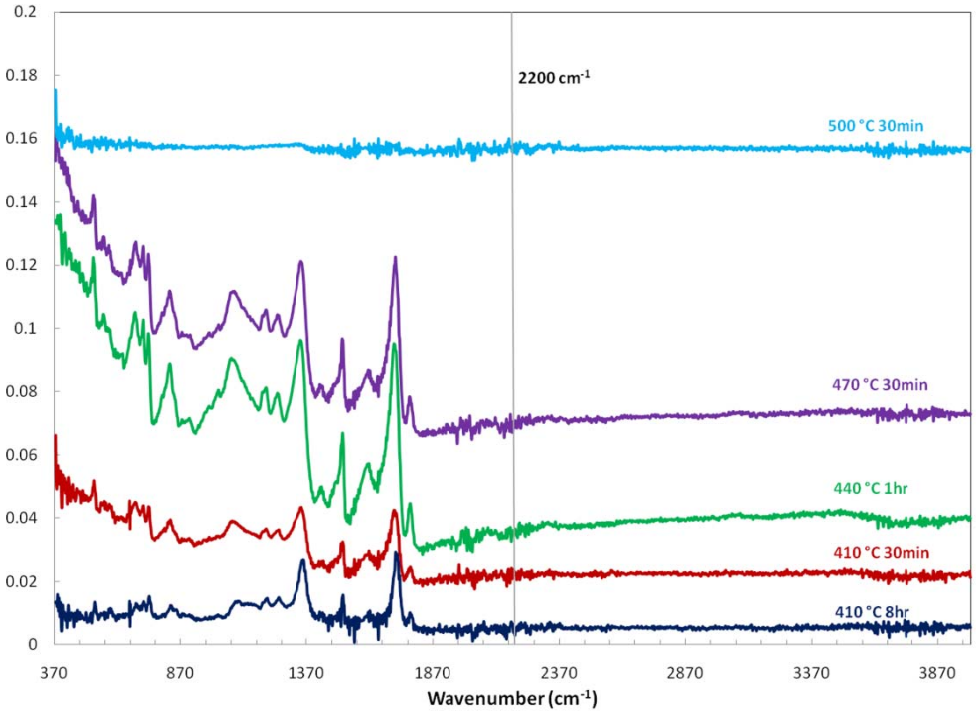

Figure 7: ATR FTIR results of further cured polyimide resin for selected cure times/temperatures.

3.2 OXIDATIVE SURFACE DEGRADATION OF COMPOSITES

The extreme service environment of hypersonic flight requires a fundamental understanding of the oxidative degradation mechanisms of both the composite resin and the carbon fiber at temperatures above 500 °C. The accelerated air diffusion from the sequential stress-induced microcrack formation of the chemically degraded brittle layers on the exterior of the material needs to be characterized.

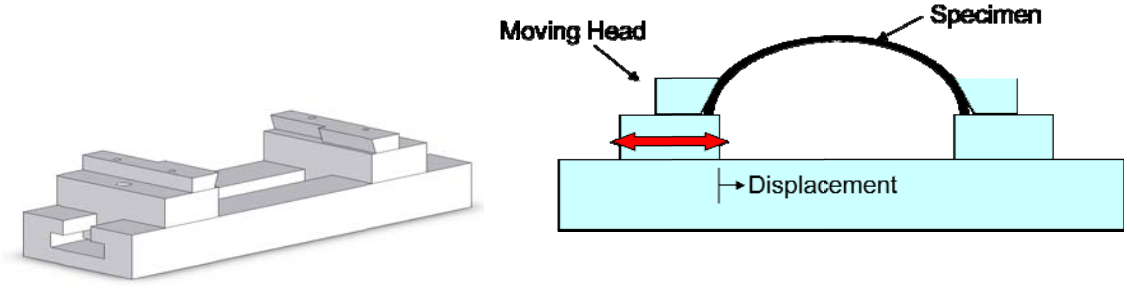

Figure 8: 3-D illustration of test fixture for oxidative degradation studies (left). Schematic of fixture with carbon fiber-polyimide composite inserted (right).

Materials being tested include: (i) AFR-PEPA-4 carbon fiber (T650-35) composite crossply 3 plies thick, (ii) AFR-PEPA-4 powder, and (iii) powdered carbon

fibers (T650-35) that have been subjected to the same air flow rate, oxygen, moisture concentration, and temperature. All the runs in air have been completed for various temperatures and air flow rates, while the runs in nitrogen are currently being completed.

3.3 COMPOSITE STRENGTH AND MODULUS

Thermal exposure can cause fiber fracture for composites that are under load, in service environment prior to any significant thermal-induced chemical or physical carbon fiber damage because of the decrease in fiber strength with increasing temperature [2]. The polyimide matrix loses its load transfer capability at its T_g that results in a loss of transverse strength of the composite layers. The loss of carbon-fiber strength with increasing temperature under load needs to be quantified for hypersonic vehicle service environments.

Testing of the AFR-PEPA-4 carbon fiber (T650-35) composites was completed over the 2008-09 winter break using an MTS frame with quartz lamps as the heating source at the desired temperature. The composites were studied from 300 to 500 °C and tested after an initial soak time of 3-5 minutes at desired temperature. The composites were characterized to show that there was a decrease in thermal-induced mechanical properties as the exposure temperature was increased. Figure 9 shows the linear decrease in tensile strength as the testing temperature was increased. The composites lost approximately one-third of their strength after exposure to 500°C. The elastic moduli exhibited the same linear decreasing trend as that of the tensile strength data; however, the composites moduli decreased by nearly half after being subjected to 500°C. There was an interesting trend observed with both the strength and modulus of the composite tested at 450°C. Both properties increased after exposure with the elastic modulus showing a more drastic improvement over the tensile strength. This occurrence could have possibly resulted from a strong interaction occurring between the polyimide resin and carbon fibers. The results obtained through this testing overall followed trends that were expected, despite the observations made at 450°C.

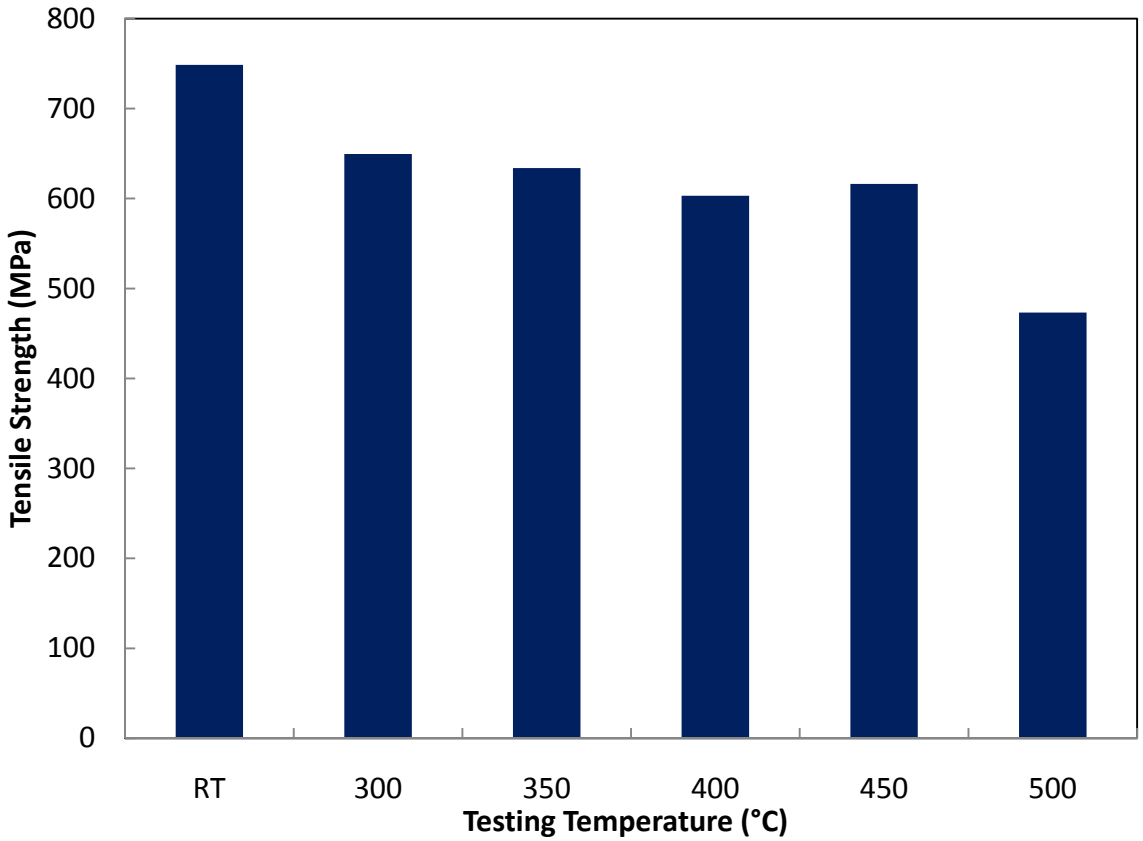

Figure 9: Polyimide carbon fiber composite's tensile strength (MPa) as a function of testing temperature (°C).

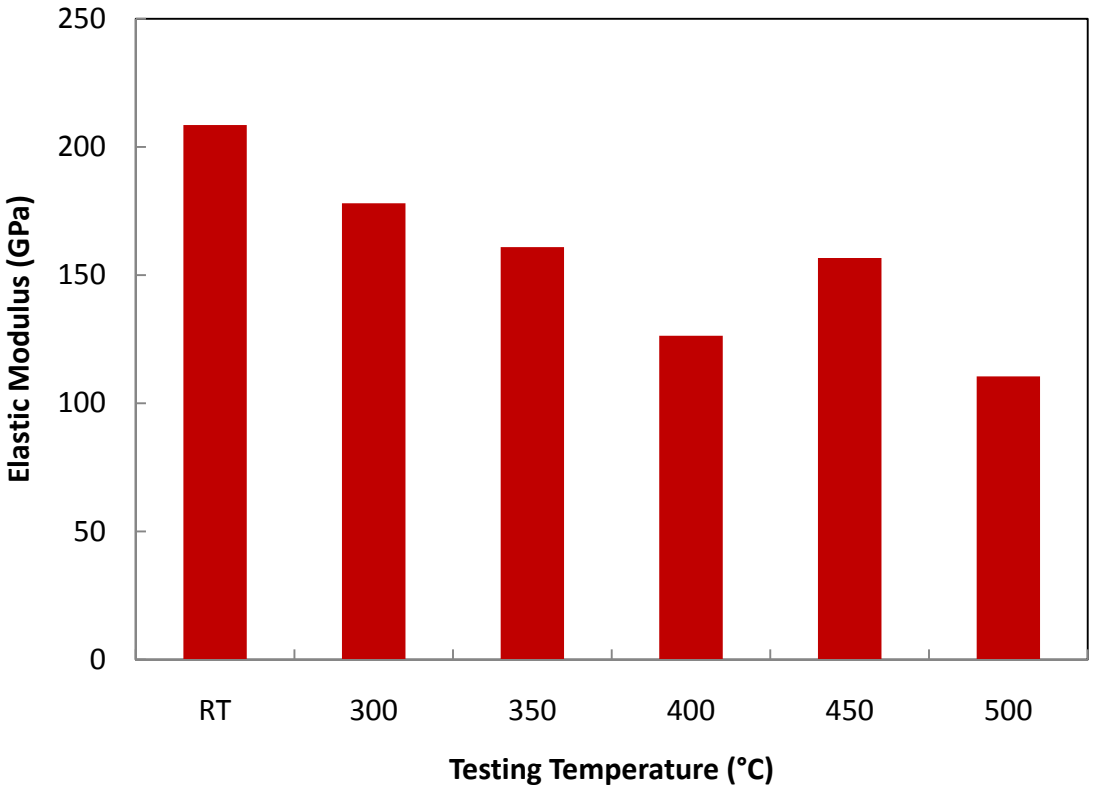

Figure 10: Polyimide carbon fiber composite's elastic modulus (GPa) as a function of testing temperature (°C).

3.4 MOISTURE-INDUCED COMPOSITE BLISTERING

The fast heating rates associated with the hypersonic vehicle service environment will not allow inherent moisture in the composite to completely diffuse and evaporate from the composite prior to the moisture vapor pressure exceeding the resin yield stress. This leads to matrix and fiber-matrix interface blistering. As a result, blister formation thresholds were determined for AFR-PEPA-4 polyimide carbon fiber composites. Composites pieces were dried in a vacuum oven before being subjected to moisture by way of a humidity controlled oven at 100 °C and 83% relative humidity. The pieces are maintained in that environment until testing to measure the dimensional change of the piece to obtain the blister temperature.

Thickness expansion was measured with a transverse extensometer equipped with quartz lamps as a heating source, as shown in Figure 11(a). A schematic of this apparatus is shown in Figure 11(b). The samples were placed on two alumina rods supported at the ends by metal stands and positioned in the center of the quartz lamps and heated to 500°C with a 50°C/min heating rate. Figure 12 shows the relatively linear relationship between blister onset and moisture content for the polyimide

carbon fiber composite samples. Moisture contents of 0.4 - 1.5 wt% resulted in blister onset temperatures of 246 - 294°C. These low onset temperatures are not surprising because composites typically have more voids and pre-existing flaws, in particular due to a weak interface between the resin and carbon fiber that lead to lower amounts of moisture causing blistering relative to the neat resin. The composite does not absorb as much moisture as the neat resin due to the large concentration (55 wt%) of non-moisture absorbing carbon fiber. Table 1 shows the amount of moisture uptake, thickness change, blister temperature, and storage modulus for the composites. While the blister temperature is affected in relation to the amount of moisture present, there is no clear relationship between the thickness change or storage modulus of the composite with respect to moisture amounts or blister temperature. The sample not subjected to moisture nor blistering conditions exhibited a storage modulus of 8333 MPa. However, the non-moisture induced/blistered sample and moisture induced/nonblistered sample resulted in storage moduli of 1442 and 2600 MPa, respectively. Therefore, a reduction in storage modulus is a result of both moisture and blistering conditions. Optical microscope and SEM images support this assertion. The polyimide composite shows a linear decrease in blister temperature as a function of moisture present. The dry composite does not show any voids or flaws in the optical microscope image (Figure 13(a)), but the SEM images clearly indicate voids within the resin and at the resin-carbon fiber interface (Figures 14(a) and (b)). In the optical micrographs (Fig. 13) the light areas are the carbon fiber, while the darker areas are the resin. The areas with alignment and orientation are the carbon fiber in the SEM images (Fig. 14). Both types of imaging clearly illustrate the degradation that occurs in the resin and at the interface between resin and fiber due to blistering. It is interesting to note that blistering also splits the carbon fiber itself in these images. This could occur as a result of resin material flowing into gaps in the carbon fiber weave during processing. Figure 13(c) is an OM image taken from the edge of a blistered sample, which reveals that the composite undergoes oxidation on the surface during heating. This is apparent due to the inability to distinguish the layers of polyimide resin and carbon fiber.

This task has been completed and will need to be extrapolated into the hypersonic vehicle heating rate ranges and the weight loss rates analyzed by the laws of momentum to ascertain if degradation conditions are produced.

Table 1. Polyimide composite parameters heating to 500°C.

Weight % Moisture	Change in Thickness (%)	Blister Onset Temperature (°C)	Storage Modulus (MPa)
0	-	-	8333
0	10.4	303	1442
0.16	-	-	2600
0.45	9.9	294	999
0.63	12.5	272	1885
0.68	10.5	274	1674
0.87	8.4	268	1768
0.88	10.4	264	1964
1.04	10.2	260	2423
1.07	8.8	261	1585
1.09	14.4	267	1486
1.21	10.8	263	1307
1.48	16.6	246	966

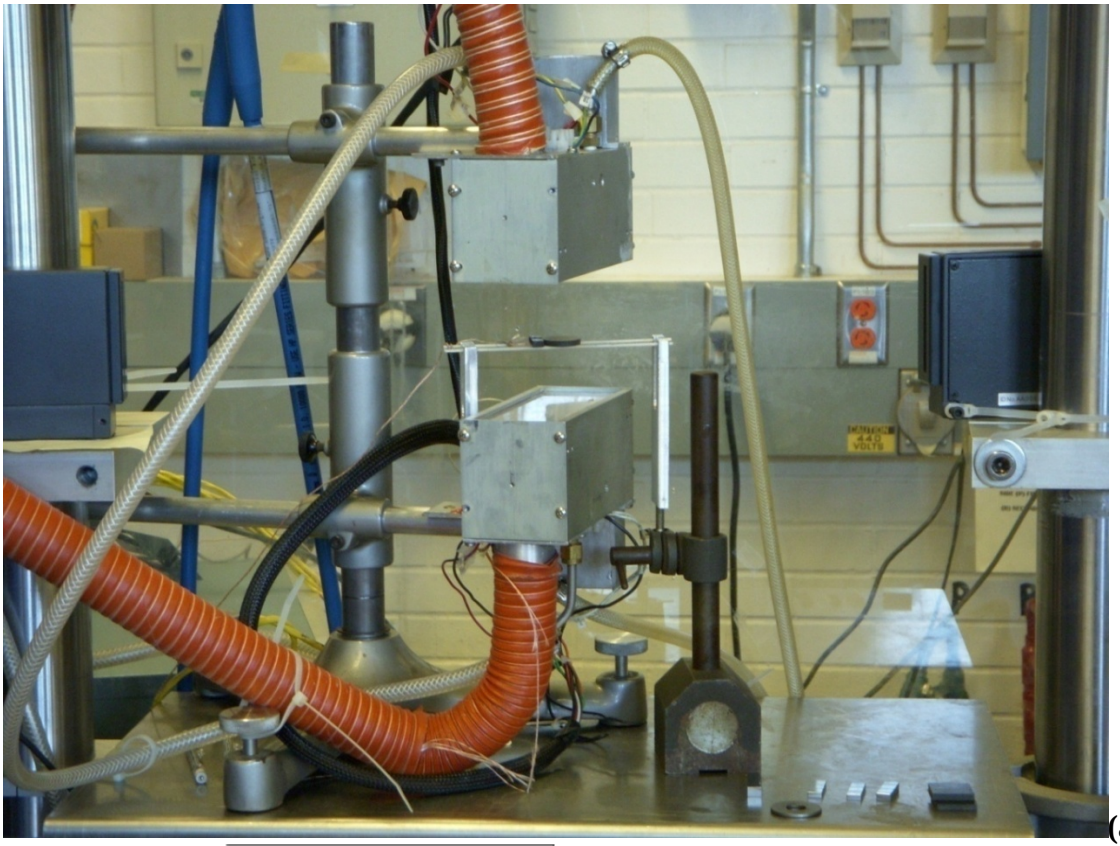

(a)

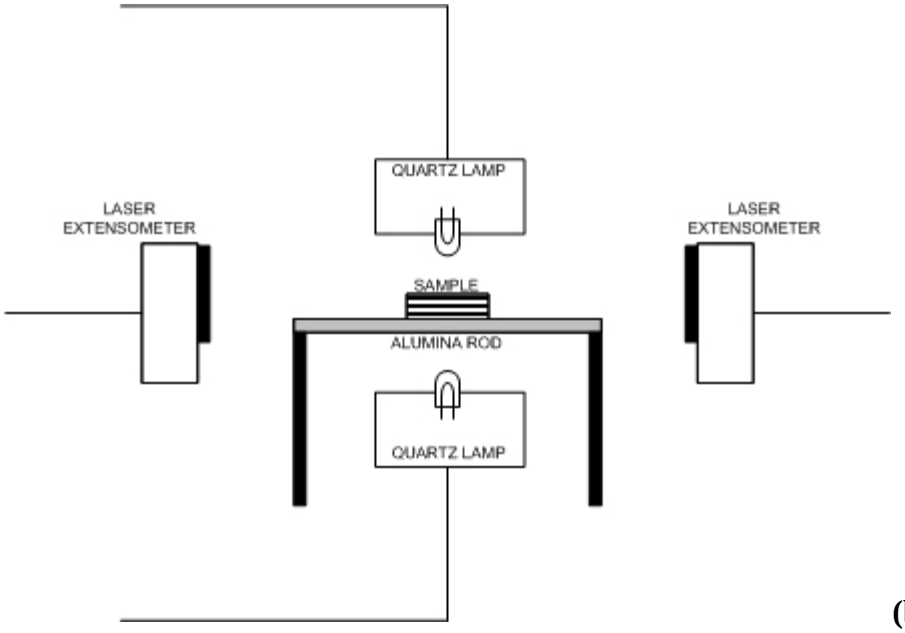

(b)

Figure 11: QUV transverse extensometer apparatus (a) for measuring dimensional changes as a function of temperature. The schematic (b) shows the key components of this device.

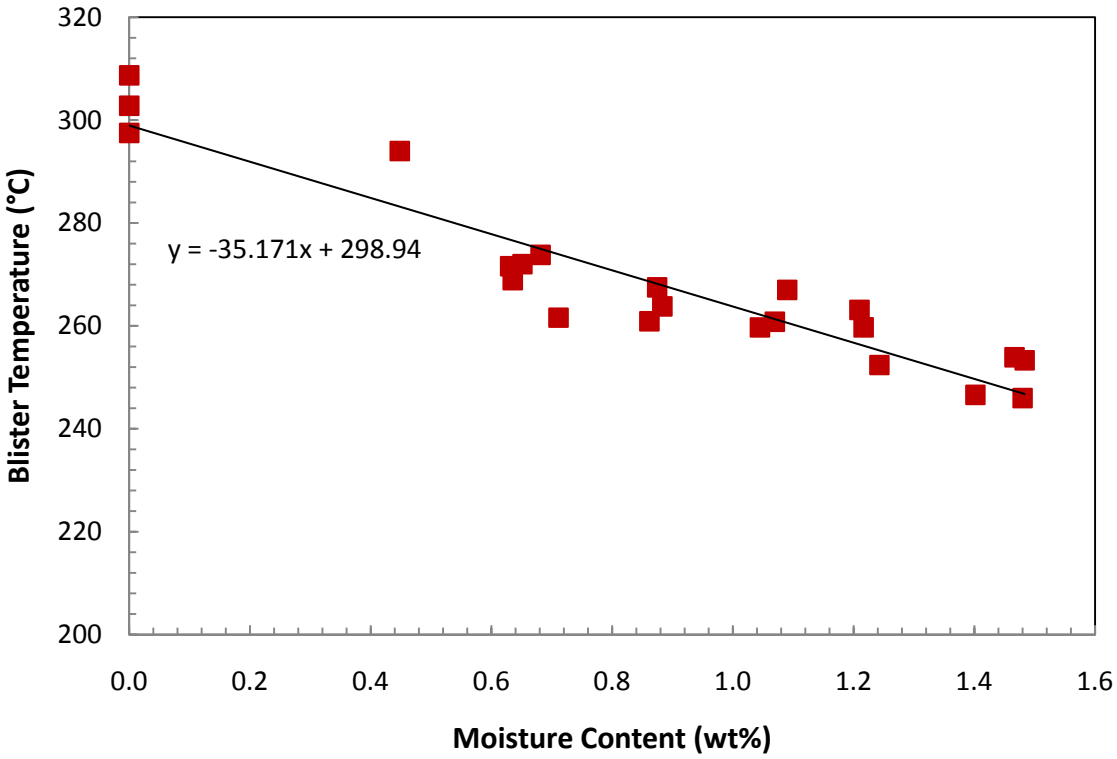

Figure 12: Temperature marking onset of blister formation as a function of moisture content in polyimide carbon fiber composite. The trendline shown has an R^2 value of 0.88.

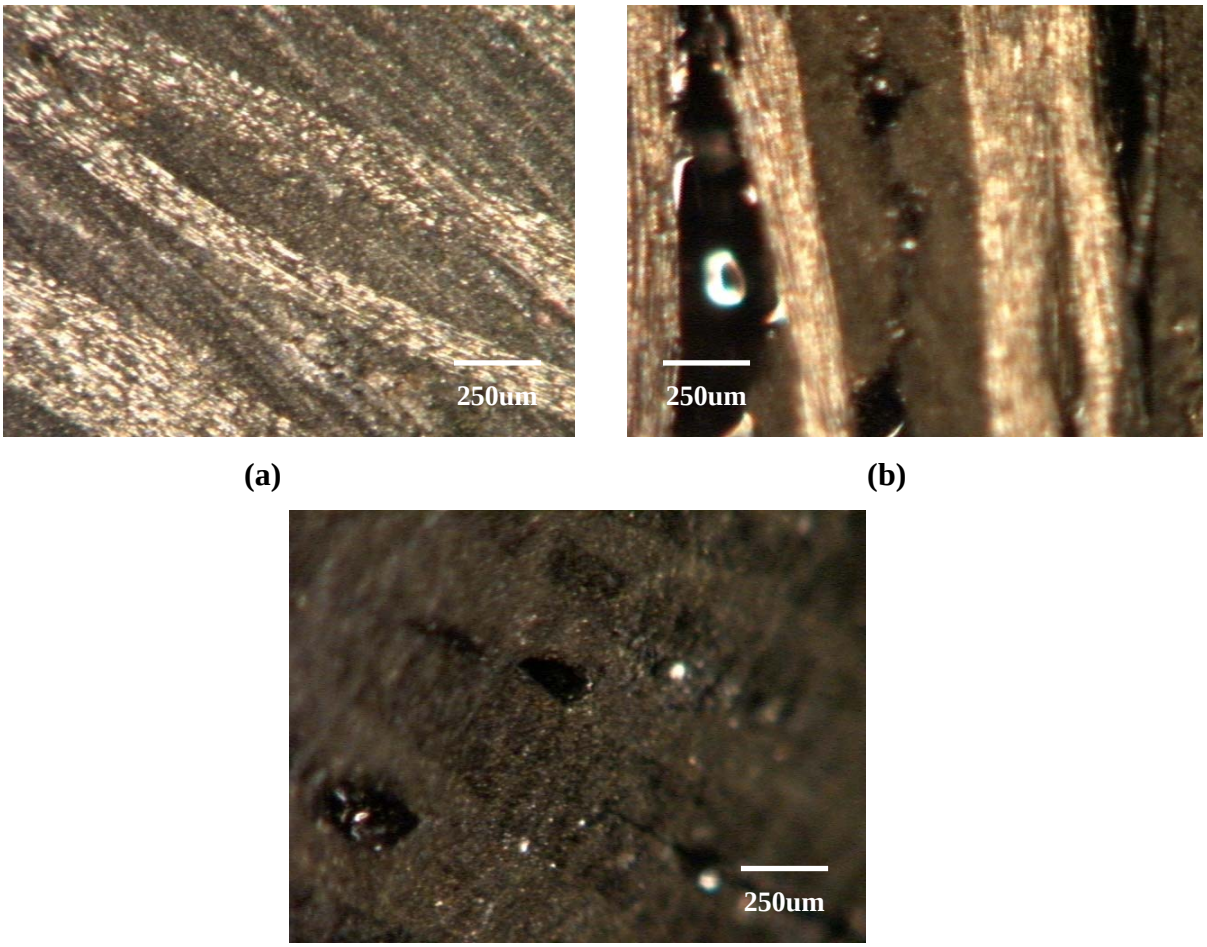

(a) **(b)**

(c)

Figure 13: Optical microscope images of the polyimide carbon fiber composite before exposure (a) and after being subjected to blister conditions (b) from inside of sample. An image taken from the edge of the composite is also shown (c).

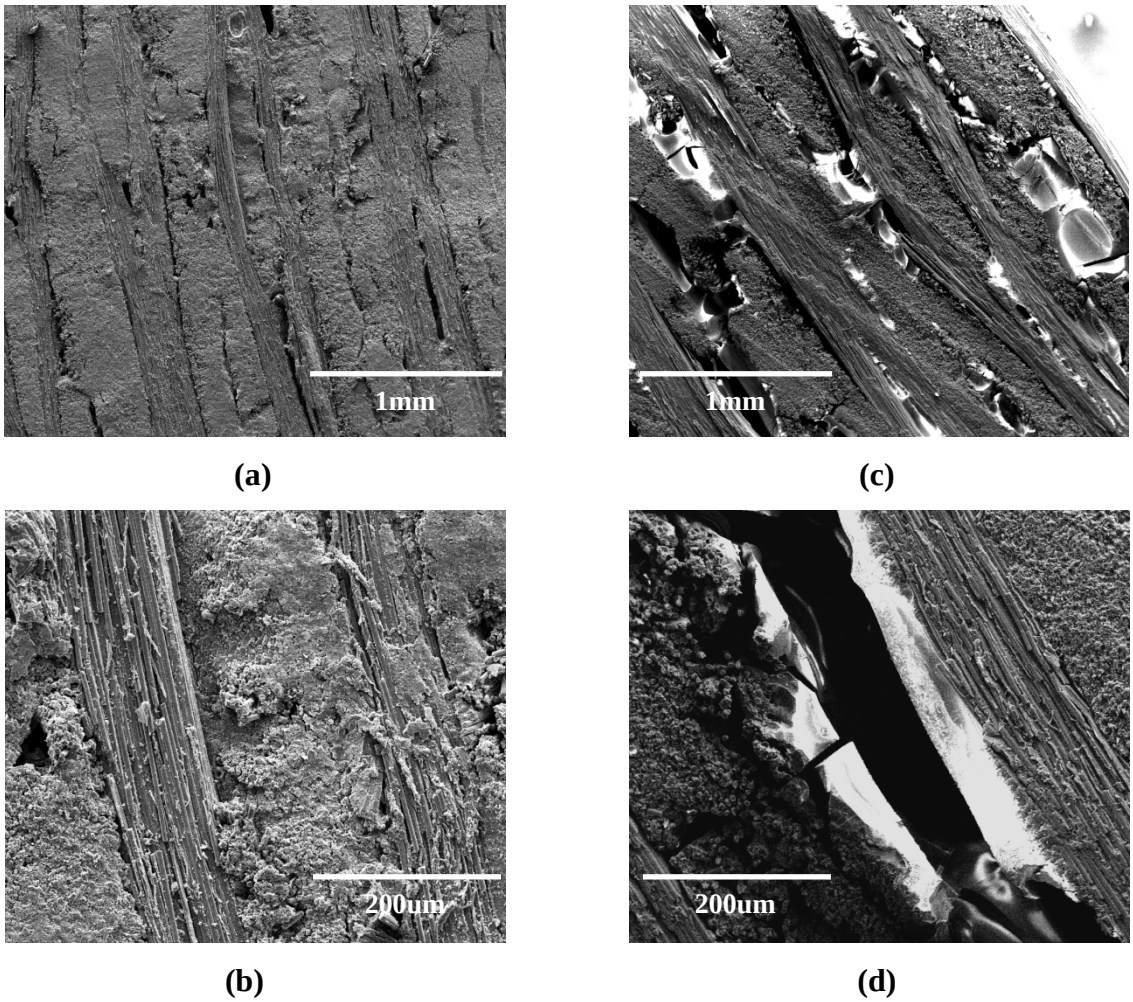

Figure 14: SEM images of polyimide carbon fiber composite before exposure ((a) and (b)) and after being subjected to blister conditions ((c) and (d)).

3.5 ABLATION/SPALLING

The rapid heating of composites in hypersonic vehicle service environments can potentially result in rapid weight loss in the form of ablation and spalling. The AFR-PEPA-4 polyimide carbon fiber (T650-35) composites were introduced into preheated air ovens at 250 - 500 °C with isothermal exposure times up to 20 minutes. Weight loss measurements were recorded as a function of temperature-time exposures.

The decomposition temperature of the polyimide containing 55 wt-% carbon fiber is 554°C. This high temperature allows the composite to withstand 510°C for up to 20 minutes and maintain weight loss below 5%. At temperatures below 470°C, weight loss is less than 1% regardless of the amount of exposure time. Figure 15(a) shows the percent weight loss as a function of temperature for the polyimide composite. At temperatures below 430°C, the weight loss is less than 1% regardless

of the amount of exposure time. Weight loss shows an exponential trend up to 510°C (see Fig. 15(a)) and is expected to continue to higher temperatures. It is not until 430°C that any significant degradation is observed, which is expected due to the thermal stability of the composite material below its decomposition temperature. When exposure temperatures are greater than 490°C the composite material begins to show signs of weight loss greater than 1% at all exposure times, as shown in Figure 15(b). This result is not surprising because the temperature is nearing the decomposition temperature. The barrier from the carbon fiber also delays the decomposition (break down) of the polyimide resin within the composite. This is supported by the optical micrographs shown in Figure 16. There is no change in the composite at the lower temperatures as seen in Figures 16(b) and 16(c). The light areas in the composite are the carbon fiber, while the darker areas are the resin. Also of interest, at 510°C, is the delayed degradation at the interface between the carbon fiber and resin in the composite (Fig. 16(e)). This observation reinforces the idea that the composite material has a strong fiber-matrix interface, thus resulting in good thermal stability. The carbon fiber in the composite also prevents structural defects from occurring at higher temperatures as seen from the images taken at 490°C (Figures 16(d)). Figure 17 shows that this strong interaction remains after exposure to 510°C for 20 minutes. These cross-sectional images of polyimide composite, exposed to 510°C for 20 minutes, show the carbon fiber tightly interfaced with the matrix. Cracks in the polyimide are very apparent at both low (Fig. 17(a)) and high (Fig. 17(b)) magnification, but no significant gaps are observed where polymer meets fiber. Very little degradation (<1% weight loss) was observed for the fluorinated polyimide carbon fiber composite, when exposed to temperatures below 430°C. Beyond 470°C, the carbon fiber-filled composite displayed relatively linear weight loss as a function of time, but this linear slope grew exponentially with temperature.

This task has been completed and will need to be extrapolated into the hypersonic vehicle heating rate ranges and the weight loss rates analyzed by the laws of momentum to ascertain if degradation conditions are produced.

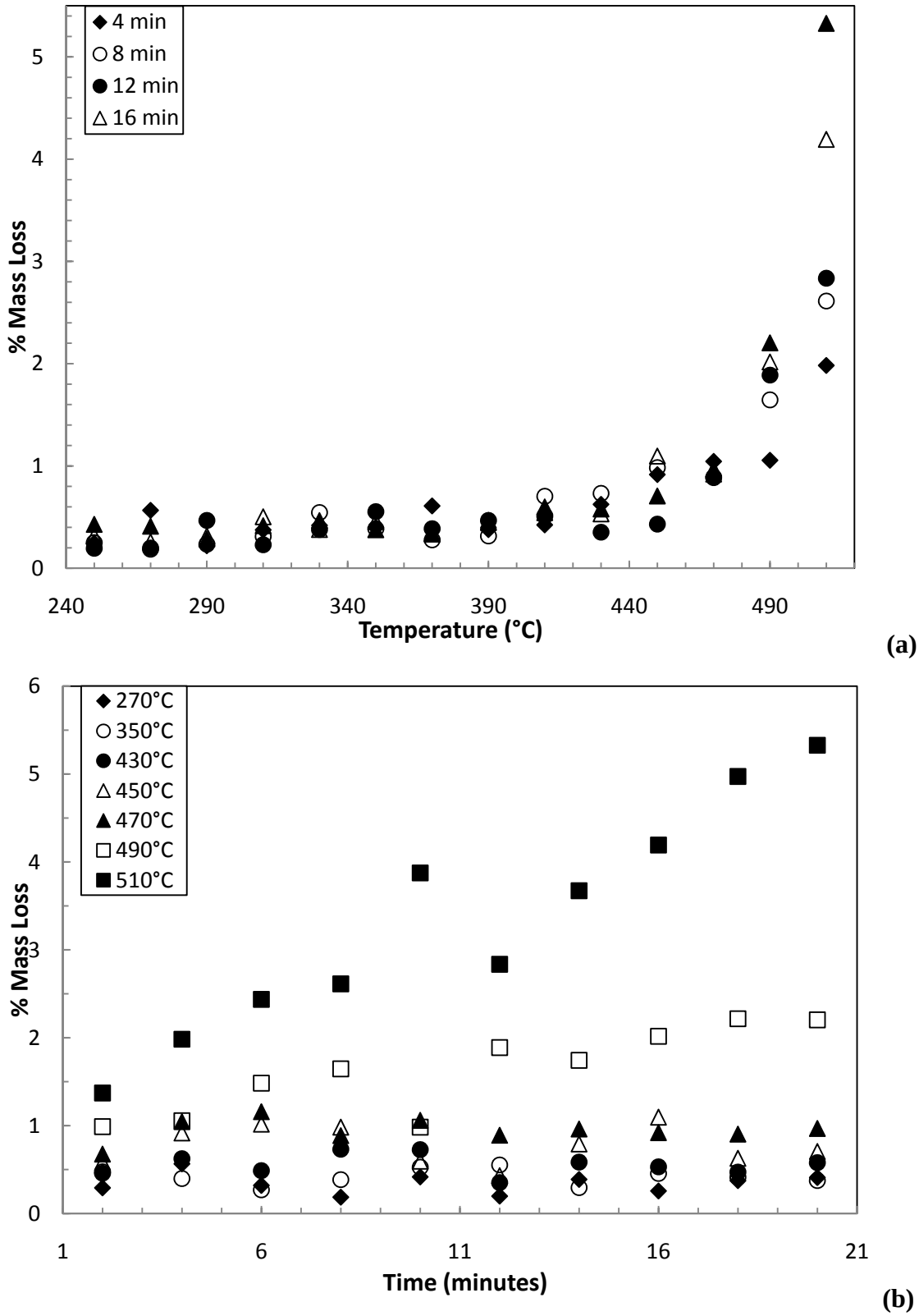

Figure 15: Polyimide composite mass loss in oven as a function of temperature (a) and time (b).

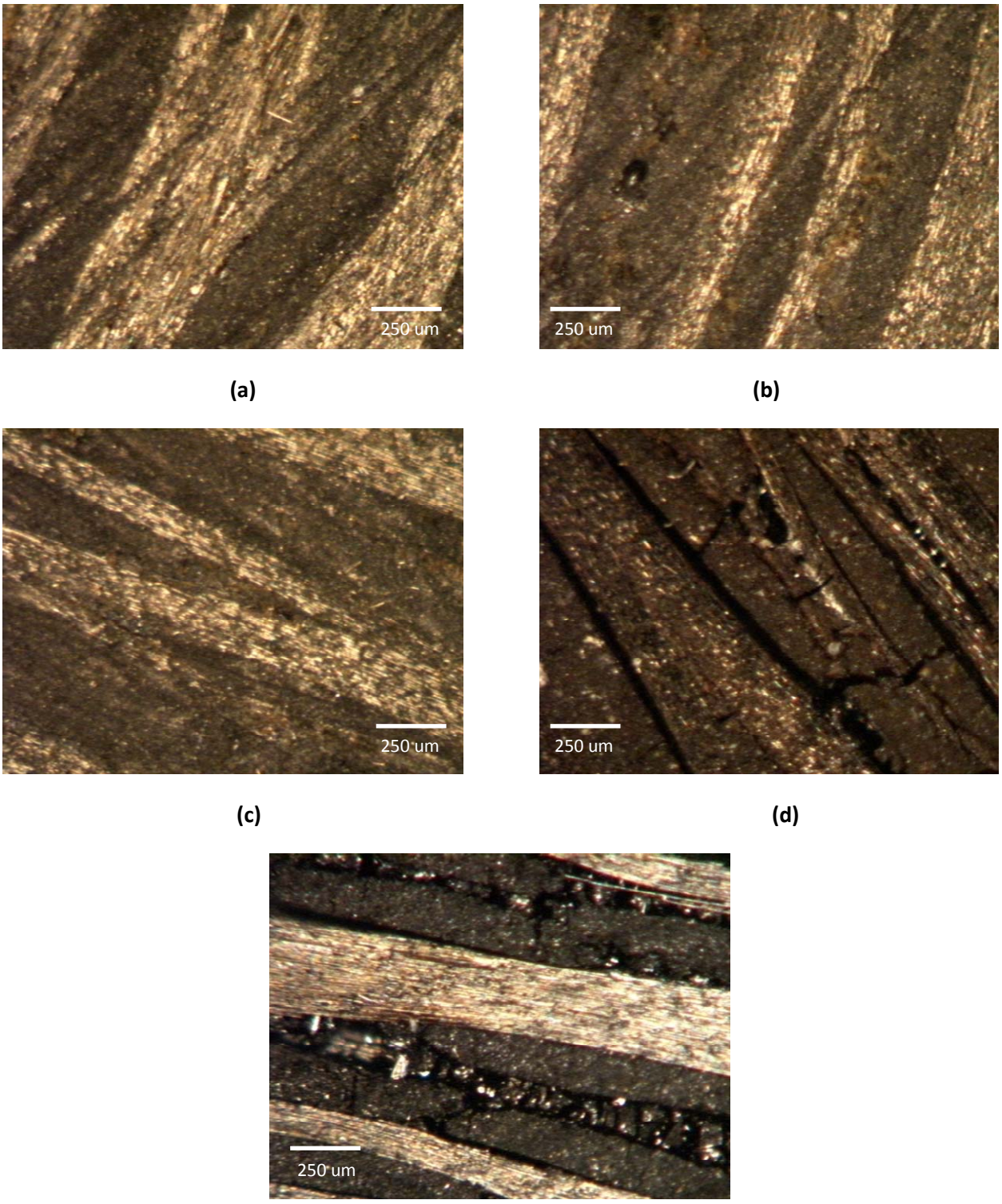

Figure 16: Optical microscope images of polyimide composite prior to ablation (a) and ablated at 250°C (b), 370°C (c), 490°C (d), 510°C (e) for 20 minutes.

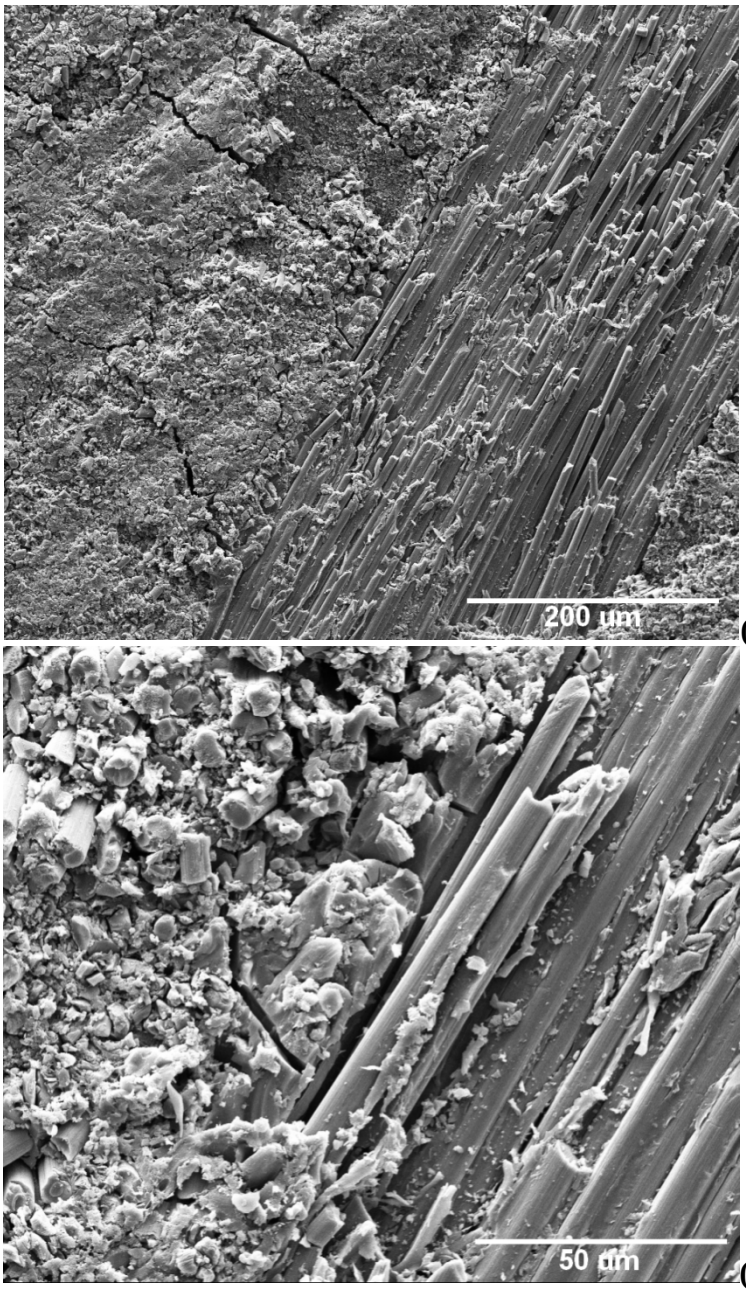

Figure 17: Scanning electron microscope images of polyimide composite cross-sections, after aging at 510°C for 20 minutes, at 500x (a) and 2000x magnification (b).

4 DAMAGE ACCUMULATION MODEL

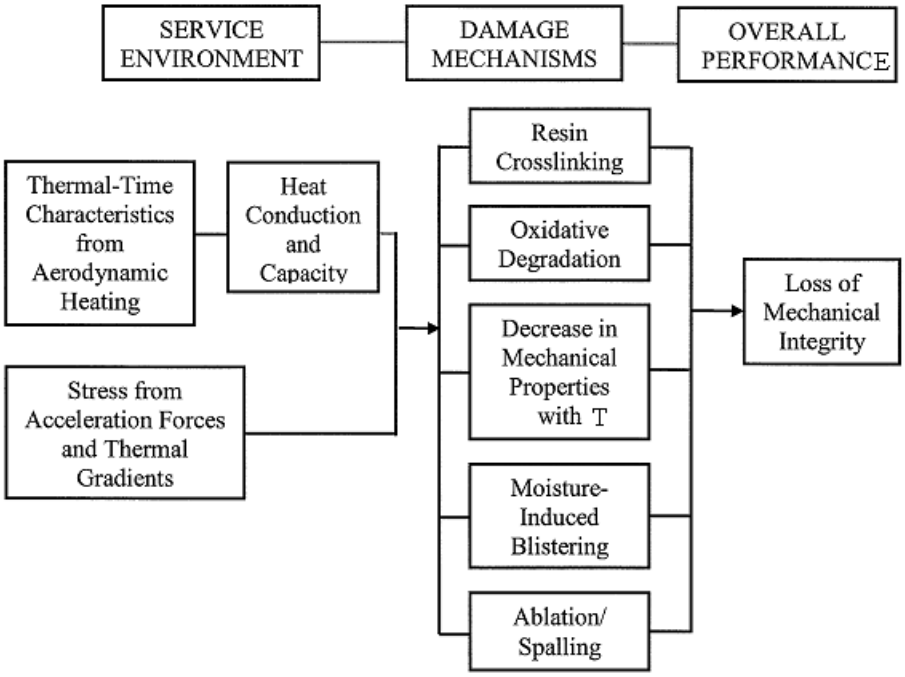

Figure 18: Future Hypersonic Vehicle Primary Structure Composite Failure Modeling

4.1 MOISTURE-INDUCED DAMAGE MODELING

In this work, we shall extend the viscolelastic solid model developed for polyimide previously to include diffusion of a Newtonian fluid (which can be, for example, moisture), using mixture theory. We also include the effects of temperature in the model developed below.

Preliminaries

We shall consider a mixture of a viscoelastic solid and a Newtonian fluid. Let us denote the quantities associated with the fluid through the superscript f and with the superscript s for that of the solid. We shall also assume co-occupancy of the constituents. Now, we shall define the motion χ^i for the i-th constituent of the mixture through

$$\mathbf{x} = \chi^i\left(\mathbf{X}^i, t\right), \quad i = f, s \tag{1}$$

where $\mathbf{X}^i$ is the material point of the i-th constituent in its reference configuration and it is assumed that the mapping χ^i is sufficiently smooth and invertible at each time t. The velocity associated with the i-th constituent is defined as

$$\mathbf{v}^i = \frac{\partial \chi^i}{\partial t}, \tag{2}$$

and the deformation gradient through

$$\mathbf{F}^i = \frac{\partial \chi^i}{\partial \mathbf{x}^i}. \tag{3}$$

The density ρ and the average velocity (also known as **barycentric** velocity) $\mathbf{v}$ of the mixture are defined by

$$\rho = \sum_i \rho^i, \quad \mathbf{v} = \frac{1}{\rho}\sum_i \rho^i \mathbf{v}^i. \tag{4}$$

We define the following derivatives for any scalar quantity ϕ^i by

$$\frac{\partial \phi^i}{\partial t} = \frac{\partial \tilde{\phi}^i}{\partial t}, \quad \frac{d^i \phi^i}{dt} = \frac{\partial \hat{\phi}^i}{\partial t}, \quad \nabla \phi^i = \frac{\partial \tilde{\phi}^i}{\partial \mathbf{x}}, \quad \frac{\partial \phi^i}{\partial \mathbf{X}^i} = \frac{\partial \hat{\phi}^i}{\partial \mathbf{X}^i}, \tag{5}$$

where

$$\phi^i = \tilde{\phi}^i\left(\mathbf{x}^i, t\right) = \hat{\phi}^i\left(\mathbf{X}^i, t\right). \tag{6}$$

Hence,

$$\frac{d^i \phi^i}{dt} = \frac{\partial \phi^i}{\partial t} + \nabla \phi^i . \mathbf{v}^i, \tag{7}$$

and we shall also define the following

$$\frac{d\phi}{dt} = \frac{\partial \phi}{\partial t} + \nabla \phi . \mathbf{v}. \tag{8}$$

The velocity gradient for the i-th component $\mathbf{L}^i$ and the velocity gradient for the total mixture $\mathbf{L}$ are defined by

$$\mathbf{L}^i = \nabla \mathbf{v}^i, \quad \mathbf{L} = \nabla \mathbf{v}. \tag{9}$$

The symmetric and anti-symmetric parts for the velocity gradients $\mathbf{L}^i$, $\mathbf{L}$ are

$$\mathbf{D}^i = \frac{1}{2}\left[\mathbf{L}^i + \left(\mathbf{L}^i\right)^T\right], \quad \mathbf{W}^i = \frac{1}{2}\left[\mathbf{L}^i - \left(\mathbf{L}^i\right)^T\right],$$
$$\mathbf{D} = \frac{1}{2}\left[\mathbf{L} + (\mathbf{L})^T\right], \quad \mathbf{W} = \frac{1}{2}\left[\mathbf{L} - (\mathbf{L})^T\right]. \tag{10}$$

The left Cauchy-Green stretch tensor $\mathbf{B}^i$ and its prinicipal invariants for the i-th constituent are defined as

$$\mathbf{B}^i = \mathbf{F}^i\left(\mathbf{F}^i\right)^T, \tag{11}$$

$$I_{\mathbf{B}^i} = \mathrm{tr}\left(\mathbf{B}^i\right), \quad II_{\mathbf{B}^i} = \frac{1}{2}\left[\left(\mathrm{tr}\left(\mathbf{B}^i\right)\right)^2 - \mathrm{tr}\left(\left(\mathbf{B}^i\right)^2\right)\right], \quad III_{\mathbf{B}^i} = det\left(\mathbf{B}^i\right), \tag{12}$$

where $det(.)$ is the determinant of a second order tensor. The above defined kinematical quantities are sufficient for the following work.

Balance Laws

We shall now note the balance laws. The balance of mass for the i-th constituent without any mass production is given by

$$\frac{\partial \rho^i}{\partial t} + \mathrm{div}\left(\rho^i \mathbf{v}^i\right) = 0, \tag{13}$$

where ρ^i is the mass density of the i-th constituent and $\mathrm{div}(.) := \mathrm{tr}(\nabla(.))$ is the divergence operator with $\mathrm{tr}(.)$ meaning the trace of a second order tensor. The summation of eqn. (13) over i leads to

$$\frac{\partial \rho}{\partial t} + \mathrm{div}\left(\rho \mathbf{v}\right) = 0. \tag{14}$$

The balance of linear momentum for i-th constituent is

$$\rho^i \frac{d^i \mathbf{v}^i}{dt} = \mathrm{div}\left(\mathbf{T}^i\right)^T + \rho^i \mathbf{b}^i + \mathbf{m}^i, \tag{15}$$

where $\mathbf{m}^i$ is the interaction force on the i-th constituent due to the other constituents, $\mathbf{b}^i$ is the external body force on the i-th constituent, $\mathbf{T}^i$ is the partial Cauchy stress tensor

associated with the i-th constituent related to the surface traction on the i-th constituent $\mathbf{t}^i$ through

$$\mathbf{t}^i = \left(\mathbf{T}^i\right)^T \mathbf{n}, \tag{16}$$

where $\mathbf{n}$ is the surface outward normal. We also have, using Newton's third law,

$$\sum_i \mathbf{m}_i = 0. \tag{17}$$

For mixtures, the balance of momentum of angular momentum, in the absence of body couples requires that the total Cauchy stress of the mixture be symmetric i.e.,

$$\mathbf{T} = \mathbf{T}^T, \quad \text{where} \quad \mathbf{T} = \sum_i \mathbf{T}^i, \tag{18}$$

although the individual partial stresses $\mathbf{T}^i$ could be non-symmetric. Now, the balance of energy for the i-th constituent is given by

$$\rho^i \frac{d}{dt}\left(\epsilon^i + \frac{\mathbf{v}^i.\mathbf{v}^i}{2}\right) = \text{div}\left(\mathbf{T}^i.\mathbf{v}^i - \mathbf{q}^\mathbf{i}\right) + \rho^i r^i + \rho^i \mathbf{b}^i.\mathbf{v}^i + E^i + \mathbf{m}^i.\mathbf{v}^i, \tag{19}$$

where ϵ^i, $\mathbf{q}^i$, r^i are the specific internal energy, heat flux, radiant heating associated with the i-th component and E^i is the energy supplied to the i-th constituent from the other constituents.

Now, taking the scalar multiplication of eqn. (15) and $\mathbf{v}^i$ and subtracting the resulting equation from eqn. (19), we arrive at

$$\rho^i \frac{d\epsilon^i}{dt} = \mathbf{T}^i.\mathbf{L}^i - \text{div}\mathbf{q}^i + \rho^i r^i + E^i, \tag{20}$$

Using $\epsilon^i = \psi^i + \theta\eta^i$, where ψ^i, η^i are the Helmholtz potential and specific entropy of the i-th constituent, with θ being the common temperature of the constituents at a point in the mixture. Next, we shall define

$$\mathbf{q} = \sum_i \mathbf{q}^\mathbf{i}, \quad r = \frac{1}{\rho}\sum_i \rho^i r^i \tag{21}$$

The balance of entropy is

$$\frac{\partial}{\partial t}\left(\sum_i \rho^i \eta^i\right) + \text{div}\left(\sum_i \rho^i \eta^i \mathbf{v}^i\right) = \frac{1}{\theta}\sum_i \mathbf{T}^i.\mathbf{L}^i - \text{div}\left(\frac{\mathbf{q}}{\theta}\right) - \frac{1}{\theta^2}\mathbf{q}.\nabla\theta + \rho\left(\frac{r}{\theta}\right) + \frac{1}{\theta}\sum_i E^i - \frac{1}{\theta}\sum_i \rho^i \left(\frac{d^i\psi^i}{dt}\right)_{\theta=constant}. \tag{22}$$

and so the rate of entropy production ζ reduces to

$$\zeta = \frac{1}{\theta}\sum_i \mathbf{T}^i.\mathbf{L}^i - \frac{1}{\theta^2}\mathbf{q}.\nabla\theta + \frac{1}{\theta}\sum_i E^i - \frac{1}{\theta}\sum_i \rho^i \left(\frac{d^i\psi^i}{dt}\right)_{\theta=constant}. \tag{23}$$

where the last term means taking derivative keeping the temperature constant. Assuming that the total entropy production can be additively split into entropy production due to thermal effects i.e., conduction (ζ_c), and entropy production due to internal working and mixing (ζ_m), we get that

$$\zeta_c := -\frac{\mathbf{q}.\nabla\theta}{\theta^2} \geq 0, \tag{24}$$

$$\zeta_m := \frac{1}{\theta}\sum_i \mathbf{T}^i.\mathbf{L}^i + \frac{1}{\theta}\sum_i E^i - \frac{1}{\theta}\sum_i \rho^i \left(\frac{d^i\psi^i}{dt}\right)_{\theta=constant} \geq 0. \tag{25}$$

Now choosing Fourier's relation for heat conduction $\mathbf{q} = -k(\rho,\theta)\nabla\theta,\ k \geq 0$, (24) is automatically satisfied. Next, defining the rate of dissipation as $\xi_m := \theta\zeta_m$, we get

$$\sum_i \mathbf{T}^i.\mathbf{L}^i + \sum_i E^i - \sum_i \rho^i \left(\frac{d^i\psi^i}{dt}\right)_{\theta=constant} = \xi \geq 0. \tag{26}$$

Assuming

$$\sum_i E^i + \sum_i \mathbf{m}^i.\mathbf{v}^i = 0, \tag{27}$$

eqn. (26) reduces to

$$\sum_i \mathbf{T}^i.\mathbf{L}^i - \sum_i \mathbf{m}^i.\mathbf{v}^i - \left[\rho\frac{d\psi}{dt} + \text{div}\left(\sum_i \rho^i\psi^i\left(\mathbf{v}^i - \mathbf{v}\right)\right)\right]_{\theta=constant} = \xi_m. \tag{28}$$

With the assumption that all the components have the same Helmholtz potential (30) leads to

$$\sum_i \mathbf{T}^i.\mathbf{L}^i - \sum_i \mathbf{m}^i.\mathbf{v}^i - \left(\rho\frac{d\psi}{dt}\right)_{\theta=constant} = \xi_m. \tag{29}$$

This is the reduced energy dissipation equation in the case of mixtures. We shall next, assume forms for the rate of dissipation and the Helmholtz potential, and then using (30) as constraint we shall maximize the rate of dissipation to get the final constitutive equations. In addition, we shall also apply the volume additivity constraint which is commonly used in mixture theory.

Constitutive assumptions

Let κ_t denote the current configuration of the mixture and let κ_R, κ_r denote the reference configurations of the solid and the fluid respectively. Also, let $\kappa_{p(t)}$ denote the natural configuration of the viscoelastic solid (see Figure 19).

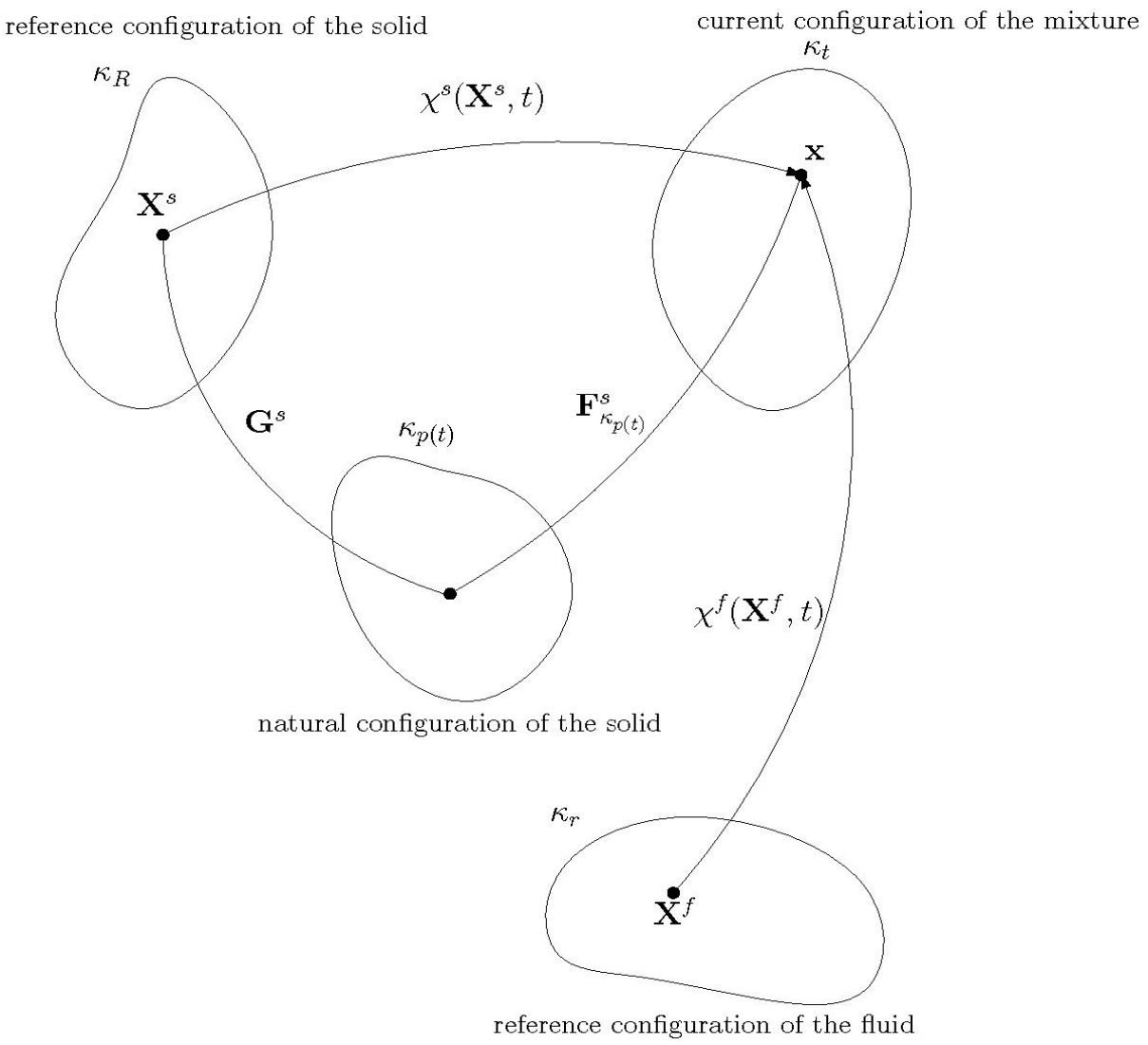

Figure 19

We shall now define

$$\mathbf{G}^s := \mathbf{F}^s \left(\mathbf{F}^s_{\kappa_{p(t)}} \right)^{-1}. \tag{30}$$

Next, we assume

$$\psi = \hat{\psi} \left(\theta, I_{B^s_G}, II_{B^s_G}, III_{B^s_G}, I_{B^s_{p(t)}}, II_{B^s_{p(t)}}, III_{B^s_{p(t)}} \right), \tag{31}$$

and it follows that

$$\dot{\psi} = 2\left[\left(\frac{\partial\hat{\psi}}{\partial I_{B_{p(t)}}} + I_{B_{p(t)}}\frac{\partial\hat{\psi}}{\partial II_{B_{p(t)}}}\right)\mathbf{B}_{p(t)} - \frac{\partial\hat{\psi}}{\partial II_{B_{p(t)}}}\mathbf{B}^2_{p(t)} - \frac{\partial\hat{\psi}}{\partial III_{B_{p(t)}}}\mathbf{I}\right].(\mathbf{L}^s - \mathbf{L}^s_G) \tag{32}$$

$$+2\left[\left(\frac{\partial\hat{\psi}}{\partial I_{B_G}} + I_{B_G}\frac{\partial\hat{\psi}}{\partial II_{B_G}}\right)\mathbf{B}_G - \frac{\partial\hat{\psi}}{\partial II_{B_G}}\mathbf{B}^2_G - \frac{\partial\hat{\psi}}{\partial III_{B_G}}\mathbf{I}\right].\mathbf{L}^s_G + \frac{\partial\hat{\psi}}{\partial\theta}\dot{\theta} + (\mathbf{v} - \mathbf{v}^s).\mathrm{grad}\psi, \tag{33}$$

We shall now note the volume additivity constraint

$$\phi^s + \phi^f = 1, \tag{34}$$

where $\phi^i = \dfrac{\rho^i}{\rho^i_R}$, $i = s, f$. Furthermore, it is assumed that the constituents are incompressible in their natural states, i.e.,

$$\rho^i_R = \text{constant}. \tag{35}$$

The balance of mass can be re-written as

$$\phi^s\mathrm{tr}(\mathbf{L}^s) + \phi^f\mathrm{tr}(\mathbf{L}^f) + \mathbf{v}^s.\mathrm{grad}\phi^s + \mathbf{v}^f.\mathrm{grad}\phi^f = 0 \tag{36}$$

Eqn. (34), we have

$$\mathrm{grad}\phi^s + \mathrm{grad}\phi^f = 0, \tag{37}$$

From (36) and (37), we get

$$\phi^s\mathrm{tr}(\mathbf{L}^s) + \phi^f\mathrm{tr}(\mathbf{L}^f) + \mathbf{v}_{s,f}.\mathrm{grad}\phi^s = 0, \tag{38}$$

where $\mathbf{v}_{s,f} = \mathbf{v}^s - \mathbf{v}^f$, is the velocity with which the fluid diffuses with respect to the solid.

We shall also assume that the rate of entropy production is of the form

$$\xi_m = \xi_m\left(\mathbf{L}^s_G, \mathbf{F}^s_{p(t)}, \mathbf{L}^f, \theta, \mathbf{v}_{s,f}\right). \tag{39}$$

The reduced energy dissipation equation reduces to

$$\mathbf{T}^s.\mathbf{L}^s + \mathbf{T}^f.\mathbf{L}^f - \mathbf{m}^s.\mathbf{v}_{s,f} - \left(\rho\frac{d\psi}{dt}\right)_{\theta=constant} = \xi_m\left(\mathbf{L}^s_G, \mathbf{F}^s_{p(t)}, \mathbf{L}^f, \theta, \mathbf{v}_{s,f}\right). \tag{40}$$

and we shall assume the specific form as follows:

$$\xi_m\left(\mathbf{L}^s_G, \mathbf{F}^s_{p(t)}, \mathbf{L}^f, \theta, \mathbf{v}_{s,f}\right) = \xi\left(\mathbf{L}^s_G, \mathbf{B}_{p(t)}, \theta\right) + \nu\mathbf{D}^f.\mathbf{D}^f + \alpha(\theta)\mathbf{v}_{s,f}.\mathbf{v}_{s,f}.$$

The first term on the RHS is the rate of dissipation due to mechanical working, the second term is the rate of dissipation due to the fluid, and the last term is the rate of dissipation due to diffusion of the fluid.

Using (33), (38) and (40), we arrive at

$$\mathbf{T}^s = -\lambda\phi^s\mathbf{I} + \mathbf{T}^s_{p(t)}, \tag{41}$$

$$\mathbf{T}^f = -\lambda\phi^f\mathbf{I} + \nu\mathbf{D}^f, \tag{42}$$

$$\mathbf{m}^s = \lambda\ \mathrm{grad}\phi^s - \alpha(\theta)\mathbf{v}_{s,f} + \rho^f\left(\mathrm{grad}\psi\right)_{\theta=constant}, \tag{43}$$

and

$$\left(\mathbf{T}^s_{p(t)} - \mathbf{T}^s_G\right).\mathbf{L}^s_G = \xi\left(\mathbf{L}^s_G, \mathbf{B}_{p(t)}, \theta\right) \tag{44}$$

where

$$\mathbf{T}^s_{p(t)} := 2\rho\left[\left(\frac{\partial\hat{\psi}}{\partial I_{B_{p(t)}}} + I_{B_{p(t)}}\frac{\partial\hat{\psi}}{\partial II_{B_{p(t)}}}\right)\mathbf{B}_{p(t)} - \frac{\partial\hat{\psi}}{\partial II_{B_{p(t)}}}\mathbf{B}^2_{p(t)} - \frac{\partial\hat{\psi}}{\partial III_{B_{p(t)}}}\mathbf{I}\right], \tag{45}$$

$$\mathbf{T}^s_{G} := 2\rho\left[\left(\frac{\partial\hat{\psi}}{\partial I_{B_{G}}} + I_{B_{G}}\frac{\partial\hat{\psi}}{\partial II_{B_{G}}}\right)\mathbf{B}_{G} - \frac{\partial\hat{\psi}}{\partial II_{B_{G}}}\mathbf{B}^2_{G} - \frac{\partial\hat{\psi}}{\partial III_{B_{G}}}\mathbf{I}\right] \tag{46}$$

Next,

$$\rho^s_R = \rho^s J^s = \rho^s J^s_G J^s_p, \tag{47}$$

where $J^s_k = det(\mathbf{F}^s_k)$, $k = G, p$ or no subscript. Assuming that there is no diffusion of mass from $\kappa_{p(t)}$ to κ_t, we have

$$J^s_G = constant \Rightarrow \frac{d^s J^s_G}{dt} = 0 \Rightarrow \mathrm{tr}\mathbf{L}^s_G = 0. \tag{48}$$

Maximizing the rate of dissipation with (52) as the constraint, we arrive at the following evolution equation for the natural configuration of the solid, given by

$$\left(\mathbf{T}^s_{p(t)} - \mathbf{T}^s_G\right) = \frac{\mu}{\beta}\mathbf{I} + \frac{\xi}{\frac{\partial\xi}{\partial\mathbf{L}^s_G}.\mathbf{L}^s_G}\frac{\partial\xi}{\partial\mathbf{L}^s_G} \tag{49}$$

Next, in order to take into account the degradation of the polyimide and the diffusion of the moisture, the following forms for the specific Helmholtz potential of the mixture

$$\hat{\psi} = A^s + (B^s + c^s_2)(\theta - \theta_s) - \frac{c^s_1}{2}(\theta - \theta_s)^2 - c^s_2\theta\ln\left(\frac{\theta}{\theta_s}\right) + \frac{\mu_{G0} - \mu_{G1}\theta}{2\rho\theta_s}(I_{B_G} - 3) + \frac{\mu_{p0} - \mu_{p1}\theta}{2\rho\theta_s}(I_{B_{p(t)}} - 3), \tag{50}$$

where $\mu_{G0}, \mu_{G1}, \mu_{p0}, \mu p1$ are elastic constants, θ_s is a reference temperature for the viscoelastic solid and the rate of dissipation ξ is of the form

$$\xi = \gamma(\theta)\mathbf{D}_G.\mathbf{D}_G, \tag{51}$$

Then, the internal energy ϵ of the solid is given by

$$\begin{aligned}\epsilon &= \psi + \theta s \\ &= A^s - B^s\theta_s + c^s_2(\theta - \theta_s) + \frac{c^s_1}{2}\left(\theta^2 - \theta^2_s\right) + \frac{\mu_{G0}}{2\rho\theta_s}(I_{B_G} - 3) + \frac{\mu_{p0}}{2\rho\theta_s}(I_{B_{p(t)}} - 3).\end{aligned} \tag{52}$$

and hence the specific heat capacity C_v is

$$C_v = -\epsilon\theta = c^s_1\theta + c^s_2. \tag{53}$$

For the form chosen in (50), we have

$$\mathbf{T}^s_{p(t)} = \frac{\rho}{\rho^s_R}\frac{J^s_p J^s_G\theta}{\theta_s}\left[\mu_p\mathbf{B}_{p(t)} - \frac{\mu_p}{2(J^s_p)^2}\left(I_{B_{p(t)}} - 3\right)\mathbf{I} - \frac{\mu_G}{2(J^s_p)^2}(I_{B_G} - 3)\mathbf{I}\right], \tag{54}$$

$$\mathbf{T}^s_{G} = \frac{\rho}{\rho^s_R}\frac{J^s_p J^s_G\theta}{\theta_s}\left[\mu_G\mathbf{B}_{G} - \frac{\mu_p}{2(J^s_G)^2}\left(I_{B_{p(t)}} - 3\right)\mathbf{I} - \frac{\mu_G}{2(J^s_G)^2}(I_{B_G} - 3)\mathbf{I}\right], \tag{55}$$

where $\mu_G = \mu_{G0} - \mu_{G1}\theta$, $\mu_p = \mu_{p0} - \mu_{p1}\theta$.

and so

$$\mathbf{T}^s = -\lambda\phi^s\mathbf{I} + \frac{\rho\theta}{\rho^s\theta_s}\left[\mu_p\mathbf{B}_{p(t)} - \frac{\mu_p}{2(J^s_p)^2}\left(I_{B_{p(t)}} - 3\right)\mathbf{I} - \frac{\mu_G}{2(J^s_p)^2}(I_{B_G} - 3)\mathbf{I}\right] \tag{56}$$

and (49) reduces to

$$\frac{\rho\theta}{\rho^s\theta^s}\left\{\mu_p\mathbf{B}_{p(t)}-\mu_G\mathbf{B}_G-\frac{1}{3}\left[\mu_p\mathrm{tr}(\mathbf{B}_{p(t)})-\mu_G\mathrm{tr}(\mathbf{B}_G)\right]\mathbf{I}\right\}=\gamma(\theta)\mathbf{D}_G \tag{57}$$

The final constitutive equations are

$$\begin{aligned}
\mathbf{T}^s &= -\lambda\phi^s\mathbf{I}+\frac{\rho}{\rho^s}\left[\bar{\mu}_p\mathbf{B}_{p(t)}-\frac{\bar{\mu}_p}{J_p^s}\left(I_{B_{p(t)}}-3\right)\mathbf{I}-\frac{\bar{\mu}_G}{J_p^s}\left(I_{B_G}-3\right)\mathbf{I}\right]\\
\mathbf{T}^f &= -\lambda\phi^f\mathbf{I}+\nu\mathbf{D}^f,\\
\mathbf{m}^s &= \lambda\ \mathrm{grad}\phi^s-\alpha(\theta)\mathbf{v}_{s,f}+\rho^f\left(\mathrm{grad}\psi\right)_{\theta=constant},
\end{aligned} \tag{58}$$

where $\bar{\mu}_p=\dfrac{\mu_{p0}-\theta\mu_{p1}}{\theta^s}$, $\bar{\mu}_G=\dfrac{\mu_{G0}-\theta\mu_{G1}}{\theta^s}$ with (57) being the evolution equation for the natural configuration of the solid.

References

1. Li, Y.; Morgan, R. J., Thermal Cure of Phenylethynyl-Terminated AFR-PEPA-4 Imide Oligomers and Their Cured Polyimides. *Journal of Applied Polymer Science* **2006,** *101*, 4446-4453.
2. Morgan, R. J.; Kong, R. M.; Lepper, J. K., Laser-Induced Damage Mechanisms of Kevlar 49-Epoxy Composites. *Journal of Composite Materials* **1988,** *22*, 1026-1044.

5 PERSONNEL SUPPORTED/ASSOCIATED

- **FACULTY**
  - Dr. K. Rajagopal
  - Dr. Jaime C. Grunlan
  - Dr. J. N. Reddy
- **POSTDOCTORAL RESEARCH ASSOCIATES**
  - Dr. Yeon Seok Kim
- **GRADUATE STUDENTS**
  - Andrea Adamczak (Ilg)
  - Satish Karra
- **UNDERGRADUATE STUDENTS**
  - Adam Spriggs
  - Danielle Fitch

PUBLICATIONS

1. Li, Y.; Morgan, R. J. Thermal Cure of Phenylethynyl-Terminated AFR-PEPA-4 Imide Oligomer and a Model Compound. *Journal of Applied Polymer Science* **2006**, *111*, 4446-4453.
2. Li, Y.; Obando, N.; Tschen, F.; Morgan, R. J. Thermal Analysis of Phenylethnyl End-Capped Fluorinated Imide Oligomer AFR-PEPA-4. *Journal of Thermal Analysis and Calorimetry* **2006**, *85*, 125-129.
3. Ju, J.; Morgan, R. J.; Shin, E. E.; Creasy, T. Characterization of Micro-cracking in M40J/PMR-II-50 under Thermal Cycling Combined with Mechanical Loading: Part I - Investigation of Main and Interactive Effects using Design of Experiment. *Journal of Composite Materials* **2007**, *41*, 1009-1031.
4. Ju, J.; Morgan, R. J.; Shin, E. E.; Creasy, T. Characterization of Micro-cracking in M40J/PMR-II-50 under Thermal Cycling Combined with Mechanical Loading: Part II – Failure Analysis. *Journal of Composite Materials* **2007**, *41*, 1067-1086.
5. Li, Y.; Murphy, L. A.; Lincoln, J. E.; Morgan, R. J. Phenylethynyl End-Capped Fluorinated Imide Oligomer AFR-PEPA-N: Morphology and Processsability Characteristics. *Macromolecular Materials and Engineering* **2007** *292*, 78-84.
6. Adamczak, A. D.; Spriggs, A. A.; Fitch, D. M.; Awad, W.; Wilkie, C. A.; Grunlan, J. C. Thermal Degradation of High Temperature Fluorinated Polyimide and its Carbon Fiber Composite. *Journal of Applied Polymer Science* **2010**, *115*, 2254-2261.
7. Adamczak, A. D.; Spriggs, A. A.; Fitch D. M.; Burke, C.; Shin, E. E.; Grunlan, J. C. Low Temperature Formation of Ultra High Temperature Transition Metal Carbides from Salt-Polymer Precursors. *Journal of the American Ceramic Society* **2010**, *93*, 2222-2228.
8. Adamczak, A. D.; Spriggs, A. A.; Fitch D. M.; Burke, C.; Shin, E. E.; Grunlan, J. C. Measurement of Blister Formation in Fluorinated Polyimide and its Carbon Fiber Composite. *Polymer Composites* **2010**, in press.
9. Karra, S.; Rajagopal, K. R. Stress Relaxation of a Generalized Neo-Hookean Solid due to Degradation. *Mechanics of Time Dependent Materials*, in review.
10. Karra, S.; Rajagopal, K. R. On the Modeling of the Viscoelastic Response of High Temperature Polyimides, in preparation.

INTERACTIONS/TRANSITIONS

(a) PARTICIPATION/PRESENTATIONS

1. Li, Y.; Murphy, L. A.; Morgan, R. J. Morphology Investigation of AFR-PEPA-N Imide Oligomer and Their Cured Polyimides. *Proceedings of 51st ISSE, SAMPE 2006*, Long Beach, CA, 2006.
2. Ju, J.; Morgan, R. J.; Shin, E. E. Transverse Interface Failure of M40J/PMR-II-50 Composites under High Temperature Exposure. *Proceedings of 51st ISSE, SAMPE 2006*, Long Beach, CA, 2006.
3. Ju, J.; Morgan, R. J.; Shin, E. E. Transverse Interface Failure of M40J/PMR-II-50 Composites under High and Low Temperature Exposure. *Proceedings of ANTEC 2006 of Society of Plastics Engineering*, Charlotte, NC, 2006.
4. Morgan, R. J.; Li, Y.; Ju, J.; Shin, E. E.; Murphy, L. A.; Obando, N. Structure-Property Relations of High Temperature Polyimide-Carbon Fiber Polymers. *Proceedings of High Temple Workshop XXVI*, Austin, TX, 2006.
5. Li, Y.; Payette, G. S.; Obando, N.; O'Neal, J.; Ju, J.; Morgan, R. J.; Reddy, J. N. Evaporative Cooling of Moisture Bearing Epoxy Composite Plate. *Proceedings of SAMPE 2006 Fall Technical Conference*, Dallas, TX, 2006.
6. Li, Y.; Tschen, F.; Lincoln, J. E.; Morgan, R. J. Structure-Property Relations of Siloxane Modified Polyimide Composites. *Proceedings of SAMPE 2006 Fall Technical Conference*, Dallas, TX, 2006.
7. Ju, J.; Morgan, R. J.; Reddy, J. N. Multiphysics Based Progressive Failure Analysis for Cryogenic Composite Fuel Tank Design. *Proceedings of ANTEC 2007 of Society of Plastics Engineering*, Cincinnati, Ohio, 2007.
8. Ilg, A. D.; Grunlan, J. C.; Spriggs, A. A.; Fitch, D. M. Analysis of Blister Formation in Fluorinated Polyimide Resin and Carbon Fiber Composites. *Proceedings of High Temple Workshop XXIX*, Napa Valley, CA 2009.

(b) CONSULTATIVE/ADVISORY FUNCTIONS

- "High Temperature Resin Performance", Jin Choi, United Technologies (By Telephone) December 2006; Jim Sutter and Eugene Shin, NASA Glenn; Fred Arnold, Greg Schoeppner Jr., AFRL, Long Beach, CA, May 2006.
- "Polyimide Composite Durability for Hypersonic Vehicles", Mike Wright, U.S. Navy-China Lake, Tom Tsotsis, Boeing, Gray Wonacolt, San Diego Composites, Andrew Facciano, Raytheon Austin, TX, February 2006.

(c) TRANSITIONS

1. (a) Morgan, TAMU; (b) Polymer Matrix Composite Lifetime; (c) NASA, Jim Sutter, Tel:216-433-3226

2. (b) Morgan, TAMU; (b) High Temperature Resin Performance; (c) Air Force Materials Directorate, Greg Schoeppner, Tel:937-255-0967
3. (a) Morgan, TAMU; (b) Ballistic High Temperature Fiber Degradation; (c) U.S. Army, Fort Belvoir, James Zheng, Tel:703-704-4865